

Dear Editor (Mathias Palm)

We submit a new version on the estimate of Paris area CO₂ emissions from the analysis of mole fraction measurements. As suggested, we do not attempt any inversion using the EIF data as input. We have nevertheless kept the model-measurement comparison to show the reader that we have a problem at the Eiffel tower. Although we could have hidden that by only using the surface station data, we feel it would be highly unethical to only show the stations that lead to positive results. We nevertheless argue that there are some specificities at Eiffel that may not impact the other stations.

The main change to the paper is that we now show a single version of the inversion. The model-measurement comparison is used to argue that (i) one should only use the stations in the near vicinity of the urban area and that (ii) only the upwind-downwind difference should be used as input. Thus, everything that was shown in section 4 is removed and we concentrate on the results that were previously in section 5 (now section 4). This makes the paper simpler and easier to read. It also fills the request by reviewer 2 of “shortening and reorganization”.

We have also reduced some of the discussion.

We hope you will agree that these changes solve the problems that were raised and that the paper in this improved form is acceptable for publication.

Best regards

An attempt at estimating Paris area CO₂ emissions from atmospheric concentration measurements

F.M. Bréon¹, G. Broquet¹, V. Puygrenier¹, F. Chevallier¹, I. Xueref-Remy¹, M. Ramonet¹, E. Dieudonné¹, M. Lopez¹, M. Schmidt¹, O. Perrussel², P. Ciais¹

[1]: {Laboratoire des Sciences du Climat et de l'Environnement, UMR CEA-CNRS-UVSQ, Gif sur Yvette, France}

[2]: {AirParif, 7 rue Crillon, Paris, France}

Correspondance to : F.M. Bréon, (breon@lsce.ipsl.fr)

Abstract

Atmospheric concentration measurements are used to adjust the daily to monthly budget of fossil fuel CO₂ emissions of the Paris urban area, from the prior estimates established by the Airparif local air quality agency. Five atmospheric monitoring sites are available, including one at the top of the Eiffel tower. The atmospheric inversion is based on a Bayesian approach, and relies on an atmospheric transport model with a spatial resolution of 2 km with boundary conditions from a global coarse grid transport model. The inversion adjusts a prior knowledge about the anthropogenic and biogenic CO₂ fluxes from the Airparif inventory and an ecosystem model, respectively, with corrections at a temporal resolution of 6 hours, while keeping the spatial distribution from the emission inventory. These corrections are based on assumptions regarding the temporal autocorrelation of prior emissions uncertainties within the daily cycle, and from day to day.

The comparison of the measurements against the atmospheric transport simulation driven by the a-priori CO₂ surface fluxes, show significant differences upwind of the Paris urban area, which suggests a large and uncertain contribution from distant sources and sinks to the CO₂ concentration variability. This contribution advocates the inversion should aim at minimizing model-data misfits in upwind-downwind gradients rather than misfits in mole fraction at individual sites. Another conclusion of the direct model-measurement comparison is that the CO₂ variability at the top of the Eiffel tower is large and poorly represented by the model for most wind speed and directions. The model inability to reproduce the CO₂ variability at the

FMB 20/1/2015 18:45	Deleted: Rémy ¹
FMB 20/1/2015 18:45	Deleted: from the AirParif inventory
FMB 20/1/2015 18:45	Deleted: . We use 5
FMB 20/1/2015 18:45	Deleted: tool
FMB 20/1/2015 18:45	Deleted: CO ₂ fluxes (
FMB 20/1/2015 18:45	Deleted:)
FMB 20/1/2015 18:45	Deleted: assuming
FMB 20/1/2015 18:45	Deleted: correlation
FMB 20/1/2015 18:45	Deleted: , while keeping the a priori spatial distribution from the emission inventory
FMB 20/1/2015 18:45	Deleted: The inversion significantly improves the agreement between measured and modelled concentrations. However, the residual misfits between the
FMB 20/1/2015 18:45	Deleted: and
FMB 20/1/2015 18:45	Deleted: model are often large compared to
FMB 20/1/2015 18:45	Deleted: measured
FMB 20/1/2015 18:45	Deleted: gradients between the sites that are used to estimate the
FMB 20/1/2015 18:45	Deleted: , in particular at the Eiffel tower station. In addition, we sometime observe large model-measurement
FMB 20/1/2015 18:45	Deleted: from
FMB 20/1/2015 18:45	Deleted: confirms the
FMB 20/1/2015 18:45	Deleted: poorly constrained
FMB 20/1/2015 18:45	Deleted: [1]
FMB 20/1/2015 18:45	Deleted: use the measured
FMB 20/1/2015 18:45	Deleted: the individual
FMB 20/1/2015 18:45	Deleted: measurements. With

heart of the city makes such measurement ill-suited for the inversion. This and the need for constraining the budgets for the whole city suggests to assimilating upwind-downwind mole fraction gradient between sites at the edge of the urban area only.

The inversion significantly improves the agreement between measured and modelled concentrations gradients. Realistic emissions are retrieved for two 30-day periods and suggest a significant overestimate by the AirParif inventory. Similar inversions over longer periods are necessary for a proper evaluation of the optimized CO₂ emissions against independent data.

1. Introduction

Although the total CO₂ emissions of developed countries may be well constrained from the total consumption of fossil fuel, its spatial and temporal distribution are not known with the same level of accuracy. In so-called bottom-up emission estimates, CO₂ emission is calculated as a combination of geo-referenced activity proxies (e.g. road traffic data, or number and type of buildings that relate to residential emissions, (Gurney et al., 2012)) multiplied by emission factors, accounting for the disaggregation of national annual budgets when dealing with regional or city inventories. The accuracy of the bottom-up inventories is seldom assessed and mostly relies on the difference between various estimates and on expert knowledge.

Due to the high population density associated with ground transportation, residence and industry, anthropogenic CO₂ emissions are large within cities (Pataki et al., 2006). The emitted CO₂ is transported in the atmosphere and results in elevated CO₂ concentration above and downwind of cities. There is therefore a potential to estimate the net CO₂ flux of a city from a few atmospheric concentration measurements located within or in the vicinity of the city (McKain et al., 2012). Over a very dense urban area, the net CO₂ flux is dominated by fossil fuel emissions, but over less dense urban structures, the net ecosystem exchange (NEE) becomes significant and can partly offset fossil CO₂ emissions during the growing season (Nordbo et al., 2012). Top-down net CO₂ flux estimates, constrained by independent atmospheric measurements, could come in complement to, or for the assessment of, current estimates that rely on bottom-up inventories.

FMB 20/1/2015 18:45
Deleted: setup, realistic

FMB 20/1/2015 18:45
Deleted: .

FMB 20/1/2015 18:45
Deleted: results

FMB 20/1/2015 18:45
Deleted: assumed or real

1 The technique of estimating surface CO₂ fluxes from atmospheric composition measurements
2 -and potentially from prior information- is relatively mature. It has been used for many years
3 to estimate the biogenic fluxes at the global (Gurney et al., 2002;Chevallier et al., 2010),
4 continental (Broquet et al., 2013;Peylin et al., 2005) and regional (Lauvaux et al.,
5 2009;Lauvaux et al., 2012) scales. However, because of uncertainties in the atmospheric
6 transport, insufficient measurement sampling, and inconsistencies between the mathematical
7 framework hypothesis of most inversions (e.g. no biases, Gaussian distribution of errors,
8 uncorrelated observation errors) and the reality, the results are not always consistent, in
9 particular at the regional scale, as shown for instance through the recent comparison of global
10 and continental-scale biogenic flux estimates by several global inversions (Peylin et al., 2013).

11 Estimating the net CO₂ flux of a city amplifies using similar mathematical and modelling
12 tools, amplifies the difficulties inherent to the atmospheric inversion. The spatial
13 heterogeneity of the source and the possibility of having very high emissions locally (e.g. a
14 power plant) make the structure of the prior error statistics complex and the concentration
15 plume highly variable. Relating mole fractions to city sources further requires accurate
16 atmospheric transport model at fine scale. Atmospheric transport in urban areas is influenced
17 by specific meteorological processes such as higher roughness of urban canopies (Zhao et al.
18 2014) and urban heat island effects (Nehrkorn et al., 2013). For instance, (Pal et al., 2012)
19 reported significantly thicker boundary layer over the Paris city than in the surrounding rural
20 area during a four day campaign that took place in March 2011, which was interpreted as a
21 consequence of the urban heat island effect. Another difficulty, shared with the inversion of
22 biogenic fluxes, lays in the temporal variability of the fossil fuel emissions, which have a
23 strong daily cycle but also day-to-day variability resulting from, for instance, temperature
24 changes (through heating) or activity (e.g. traffic) variability. Last, measurements in and
25 around a target city collect CO₂ molecules of various origins that must be separated into city
26 sources and remote sources and sinks through the inversion.

27 This challenge has been addressed recently by several research projects, e.g. INFLUX
28 (sites.psu.edu/influx, (Shepson et al., 2011)) over Indianapolis city or Megacities
29 (<http://megacities.jpl.nasa.gov>; (Duren and Miller, 2012)) over Los Angeles, which have set-
30 up a network of surface, tower and airborne measurements of the atmospheric CO₂ mole
31 fractions. Satellite data may also provide valuable information as shown by (Kort et al.,
32 2012). The results from the on-going urban CO₂ measurement project at Salt Lake City

FMB 20/1/2015 18:45

Deleted: ...)

FMB 20/1/2015 18:45

Deleted: a

FMB 20/1/2015 18:45

Deleted: groups

FMB 20/1/2015 18:45

Deleted: Although the

FMB 20/1/2015 18:45

Deleted: are similar, estimating the net CO₂ flux of a city

FMB 20/1/2015 18:45

Deleted: emission fluxes

FMB 20/1/2015 18:45

Deleted: non Gaussian

FMB 20/1/2015 18:45

Deleted: an

FMB 20/1/2015 18:45

Deleted: Indeed,

FMB 20/1/2015 18:45

Deleted: can have a complex link with the

FMB 20/1/2015 18:45

Deleted: canopy

FMB 20/1/2015 18:45

Deleted: implicitly identified

FMB 20/1/2015 18:45

Deleted: the

FMB 20/1/2015 18:45

Deleted: analyses of an

1 indicated that monthly emission relative changes of 15% could be detected at the 95%
2 confidence level with the current monitoring system (McKain et al., 2012) even though this
3 study concluded on the inability to derive absolute estimates for a given month.

FMB 20/1/2015 18:45

Deleted: despite

FMB 20/1/2015 18:45

Deleted: (McKain et al., 2012).

4 The CO₂-MegaParis project has a similar objective for the Paris area. This is a potentially
5 favourable case as the city is very dense and the emissions intense over a limited surface, with
6 a fairly flat topography in the surroundings, which makes the atmospheric transport modelling
7 easier. A pilot campaign early 2010 was conducted in the framework of the MEGAPOLI
8 project. Measurements of the mole fraction of CO₂ and its isotopes have been used to
9 estimate the relative contribution of fossil and biogenic emissions in the concentration
10 gradients (Lopez et al., 2013). The main campaign started in August 2010 with the
11 installation of three CO₂ and CO monitoring stations within the city and its surrounding that
12 provided near-continuous measurements until July 2011. These three stations complement
13 two stations of the ICOS France network located in the Paris region outside the city that have
14 been operational for several years. (Lac et al., 2013) made a first analysis of the
15 measurements and a comparison against atmospheric modelling using the Meso-NH
16 mesoscale transport model, combined with a surface scheme that accounts for the urban
17 environment, for a period of 5 days in March 2011. They demonstrated the ability of the
18 modelling framework to reproduce several features of the mixing layer height, as reported in
19 (Pal et al., 2012), and of the mole fraction daily cycle.

FMB 20/1/2015 18:45

Deleted: and of the mixing layer height

20 Large efforts have been made by AirParif, the air quality agency for the Paris area, to generate
21 an inventory of the Paris area emissions, for various pollutants and for CO₂ as well. The
22 AirParif emission inventory, detailed in section 2.2, provides an hourly description of the CO₂
23 emissions at ≈ 1 km resolution for representative weekdays and months. We use this
24 inventory as an input to the atmospheric transport simulations and compare the results to the
25 atmospheric concentration measurements from the five sites. We then attempt a correction of
26 the inventory based on the differences between the observed and modelled mole fractions.
27 With only 5 stations in the vicinity of the city, there is likely not enough information to
28 constrain the spatial distribution of the emissions. We therefore only rescale the emissions,
29 relying on the spatial distribution provided by the Airparif inventory. For the inversion, NEE
30 and fossil fuel emissions are optimized separately. We focus on two 30-day periods in the fall
31 of 2010. This choice is driven by the expectation of rather small biogenic fluxes during this
32 time period, which makes easier the interpretation of the measurements in terms of

1 anthropogenic fluxes. Our objective is to assess whether a reliable estimate of the emissions
2 [at the daily to monthly time scales](#) can be derived from the combination of atmospheric
3 measurements, available inventories and information on the atmospheric transport. A
4 forthcoming paper will apply the methodology to a full year of observations and analyse the
5 result for the spring and summer periods, when CO₂ uptake by NEE can partially offset fossil
6 fuel emissions (Pataki et al., 2007). In the following, section 2 analyses the time series of
7 measured and modelled CO₂ mole fractions; section 3 describes the methodology to correct
8 the inventory based on the measurement-model mismatches. The results are shown in section
9 [4](#) [while section 5](#) discusses the results and concludes.

10 2. Measurements and direct simulations

11 2.1. CO₂ concentration measurements

12 In this paper, we use CO₂ mole fraction measurements that have been acquired continuously
13 in the framework of the CO₂-Megaparis and ICOS-France projects. Three stations have been
14 equipped with high precision CO₂/CO analysers (Picarro G1302) specifically for the project
15 objectives. One is located in the heart of Paris, at the summit of the Eiffel tower, 300 m
16 above the surface. Two are located in the North and North-East of the Paris area in a mixed
17 urban-rural environment. They are complemented by two ICOS-France stations that were
18 operational before the start of the project. One is located in the South-West, about 20 km
19 from the centre of Paris, while the other is a tall tower located further south by about 100 km.
20 Both use gas chromatograph analysers (Agilent HP6890). The location of the stations are
21 given in Table 1 and shown in Figure 1. They are very roughly located along a NE-SW
22 direction, which defines [the dominant](#) wind directions, [thus favourable](#) for the monitoring of
23 the [CO₂ increase due to the](#) emissions [of the Paris area](#), with a station at the edge of the urban
24 area in both directions. The measurements are quality-controlled and binned at a temporal
25 resolution of 1 hour. They have been regularly calibrated against the WMO mole fraction
26 scale (Zhao and Tans, 2006) so that measurement accuracy to the WMO-X2007 scale is
27 estimated to be better than 0.38 ppm. The instrumental reproducibility is better than 0.17
28 ppm on the 5 minute average measurements available from the CO₂-Megaparis stations, [and](#)
29 the temporal averaging to the hourly-mean values used in this paper leads to precision much
30 better than the accuracy (Zhao and Tans, 2006).

FMB 20/1/2015 18:45

Deleted: and

FMB 20/1/2015 18:45

Deleted: , using two different inversion setups. Section 6

FMB 20/1/2015 18:45

Deleted: favourable

FMB 20/1/2015 18:45

Deleted:

FMB 20/1/2015 18:45

Deleted: from this observation network

FMB 20/1/2015 18:45

Deleted: but

2.2. Atmospheric transport modelling

Atmospheric transport modelling provides the link between the surface fluxes and the atmospheric mole fractions. Here, we use the Chimere transport model (Menut et al., 2013) with a resolution of 2 km around the Paris city, and 10 km for the surrounding of the modelling domain (see Figure 1). There are 118x118 pixels in the modelling grid that covers an area of approximately 500x500 km². There are 19 layers on the vertical, from the surface to 500 hPa. The Chimere transport model is driven by ECMWF-analysed meteorology at 15 km resolution. There is no urban scheme in the atmospheric modelling that is used here, which may be seen as a significant limitation to our inversion set-up. However, we conducted forward simulation comparisons between our modelling and that used in (Lac et al., 2013), which includes specific surface parameterization to account for the urban area, and we did not find significant differences on the simulated CO₂ mole fractions.

The model simulates the mole fractions that are driven by the surface fluxes and the boundary conditions. The surface fluxes that are accounted for in the simulations are the sum of

- Anthropogenic fossil fuel CO₂ emissions within the Île-de-France region, from the AirParif inventory, as described in section 2.3 and shown in Figure 2. Île-de-France is the administrative region spreading typically within 60 km around the Paris city, the boundaries of which are shown in Figure 1.
- Anthropogenic fossil fuel CO₂ emissions outside the Île-de-France region, according to the Edgar database [Edgar, 2011] available at 10 km resolution. These are only annual mean fluxes, and there is no description of the diurnal or seasonal cycle in this inventory.
- Biogenic fluxes from the C-TESSEL land surface model, as described in section 2.4.

The CO₂ boundary conditions prescribed at the lateral and top edges of the simulation domain, and transported inside the domain by Chimere, are obtained from the Monitoring Atmospheric Composition and Climate (MACC) global inversion, v10.2) (<http://www.copernicus-atmosphere.eu/>). In this simulation, the global distribution of surface CO₂ fluxes has been optimized to fit the mole fractions measured at a number of stations distributed over the world, given their assigned uncertainty and prior information of the surface fluxes. Given the relatively coarse spatial resolution of the transport model used in

FMB 20/1/2015 18:45

Deleted: does use

FMB 20/1/2015 18:45

Deleted: emission

FMB 20/1/2015 18:45

Deleted: 2.3

FMB 20/1/2015 18:45

Deleted: have

FMB 20/1/2015 18:45

Deleted: given some

FMB 20/1/2015 18:45

Deleted: underlying

1 the MACC inversion, CO₂ boundary conditions here are temporally and spatially very smooth
2 and have little impact on the spatial gradients simulated within the domain area.

3 2.3. AirParif Inventory

4 The AirParif air quality agency (<http://www.airparif.asso.fr/en/index/index>) has developed an
5 inventory of emissions (for greenhouse gases such as CO₂ but also [for](#) air pollutants) at 1 km
6 spatial resolution and hourly time step for the Île-de-France region. The emissions are
7 quantified by activity sectors. The improvement of methodologies and emission factors lead
8 to frequent updates of the emission estimates.

9 Nearly eighty different source types are included in the inventory with three main classes:
10 point sources, linear and diffuse sources. Point sources correspond to large industries, power
11 plants, and [waste](#) burning; linear sources are related to transportation, while diffuse sources
12 are mostly associated to the residential and commercial [sectors](#). The road traffic emission
13 estimates use a traffic model and vehicles counting devices that report the number of vehicles
14 and their average speed over almost 40 000 km portions of roadways. Large industries are
15 requested to report their CO₂ emissions and these are used in the inventory. For smaller
16 industrial sources that are not required to report their emissions, a disaggregation of the
17 regional fuel consumption is made based on the number of employees, leading to larger
18 uncertainties. We have used the latest available version of the inventory, corresponding to
19 year 2008, which has been developed for 5 typical months (January, April, July, August, and
20 October) and three typical days (weekday, Saturday and Sunday) to account for the seasonal
21 and weekly cycle of the emissions. Therefore this inventory estimates typical emissions but
22 does not attempt to reproduce the daily variations resulting from specific meteorological
23 conditions, or specific events such as [public holidays](#).

24 Figure 2 shows an example of the spatial distribution of the total emissions for a weekday in
25 October. Typical values are a few hundred gCO₂ m⁻² day⁻¹ within the city and a few tens
26 gCO₂ m⁻² day⁻¹ in the suburbs. The main roads are clearly shown with flux enhancements of a
27 few tens gCO₂ m⁻² day⁻¹, at the 1 km² resolution of the inventory. Further processing of this
28 map shows that one third of the Île-de-France emissions are within 10 km of the Paris centre,
29 and 61% are within 20 km.

30 There is a large temporal variation of emissions, as shown in Figure 3, mostly at the daily
31 scale, but also at the weekly and seasonal scales. Most components show a large daily cycle
32 with minimum emissions at night. During the day, the traffic related emissions show several

FMB 20/1/2015 18:45

Deleted: trash

FMB 20/1/2015 18:45

Deleted: sector

FMB 20/1/2015 18:45

Deleted: activities

FMB 20/1/2015 18:45

Deleted: vacation days

maxima, in the morning, midday, and late afternoon. The daily cycles of the other activities are less pronounced but nevertheless significant. Point sources have the smallest daily cycle amplitude due to the industrial temporal profile that is relatively flat. The Paris area has few point sources and they contribute to typically 20% of the total emissions. The seasonal cycle is most pronounced for the residential emissions related to heating and cooking. One notes that residential CO₂ emissions do not go to zero during the summer months, because energy is still consumed for cooking and for heating water in summer.

In the following, the AirParif inventory for year 2008 is used as a prior estimate of the fossil fuel emissions within the Île-de-France region, both for the direct transport simulations (section 2.5) and for the flux inversion (section 3). Note that the inventory of point source emissions provides injection heights that have been used in the source term of the simulations. The AirParif inventory is provided as a function of legal time, and we have accounted for the time shift between legal time and UTC time, including the impact of daylight saving. Note that, due to the longitude of Paris, UT time and solar times are very similar.

2.4. Biogenic Fluxes

The Net Ecosystem Exchange fluxes used here are provided by the land surface component of the ECMWF forecasting system, C-TESSEL (Boussetta et al., 2013). They are extracted from the ECMWF operational archives at the highest available resolution, 15 km and 3 hours. These data are interpolated in space (2 to 10 km) and time (1 hour) to be consistent with our [atmospheric transport](#) model grid and temporal resolution.

Figure 4 shows the mean daily cycle of NEE for the Île-de-France area and for the 12 calendar months. There are large diurnal and seasonal NEE cycles. The flux is positive (emission) during the night and negative (uptake) during the day, even during the winter months, given the rather mild winter temperature prevailing over the Paris area. Nevertheless, the amplitude of the daily cycle of NEE is much larger in summer than it is in winter. The NEE values are of similar magnitude than the anthropogenic emissions with a strong anti-correlation on the daily cycle (negative NEE vs. large anthropogenic emissions during daytime; positive NEE and smaller anthropogenic emissions during the night). During the winter, NEE is relatively small and the anthropogenic emissions clearly dominate, but daytime NEE still offsets on average ~20% of the emissions, according to the C-TESSEL model simulations. During spring and summer, however, the daytime NEE uptake is larger in absolute value than the anthropogenic emissions as shown through a comparison of Figures 3 and 4.

1 | As our main interest is the anthropogenic emissions, we chose to analyse a period when the
2 | biogenic flux is small, i.e. during fall and winter. The present paper focuses on two 30-day
3 | periods that start on October 21st and November 27th 2010. During these periods, the monthly
4 | mean hourly NEE fluxes are less than 3 ktCO₂ per hour over the Île-de-France area. NEE is
5 | then small, but not negligible, compared to anthropogenic emissions during the chosen
6 | inversion [periods](#).

7 | 2.5. Direct CO₂ transport simulations

8 | Figure 5, together with Figure S-1 in the supplementary, shows the time series of the CO₂
9 | mole fractions together with an indication of the modelled wind speed and direction to help
10 | the interpretation of the results. These time series are derived from observations and direct
11 | atmospheric modelling as described in section [2.2](#).

12 | The Trainou (TRN) station (bottom row) is far from the Paris agglomeration. In addition, the
13 | measurement inlet is at 180 m from the surface. It shows a diurnal cycle amplitude that is
14 | much smaller than at the other sites. In addition, the modelled contribution from both
15 | anthropogenic and biogenic fluxes within the simulation domains is limited to a few ppm, as
16 | shown by the difference between the black and green curve. There are a few exceptions
17 | however, essentially when the wind blows from the North, i.e. from the Paris city [direction](#),
18 | and transports [fossil CO₂ from the urban area](#) to the TRN rural site. The best examples are
19 | around Dec 8th and Dec 23rd. For these particular cases, the measurements at TRN are
20 | significantly larger than the model results. The underestimate by the model is not limited to
21 | these dates and there are significant discrepancies between the model and the measurements at
22 | this [remote](#) background site, in particular at the end of November and at the beginning of
23 | December.

24 | The other sites are much closer to Paris and are then more affected by the fossil CO₂
25 | emissions. At Gif-sur-Yvette (GIF) the largest mole fractions are observed when the wind is
26 | from the North-East, which is expected as the Paris city is in that direction. There is also an
27 | impact of the wind, as the largest mole fractions are measured in low wind speed conditions.
28 | During the Oct-Nov period (Figure S-1), the wind is mostly from the South and South-West,
29 | thus not from the city, and there is a relatively good agreement between the modelled and
30 | measured mole fractions. In December, the wind direction is more variable, the fossil CO₂
31 | signal appears much larger, and there are very significant differences between the
32 | measurements and the model estimates.

FMB 20/1/2015 18:45

Deleted: The comparison of biogenic and anthropogenic fluxes over the Île-de-France area shows that they are of similar magnitude during spring and summer. The limited number of stations installed during the CO₂-MEGAPARIS campaign is likely insufficient to properly distinguish their respective contributions, and there are significant uncertainties on the biogenic fluxes.

FMB 20/1/2015 18:45

Deleted: period

FMB 20/1/2015 18:45

Deleted: 2.4.

1 Gonesse (GON) is located to the North of the city, while Montgé-en-Goële (MON) is further
2 away to the North-East. The shorter distance to the main source may explain the larger signal
3 at the former station. The only cases when the modelled anthropogenic contribution is small
4 at GON (small difference between black and green curve) is when the wind is from the North.
5 For other wind directions, the modelled signal is strong -more than 10 ppm- and there are
6 large differences between the measurements and the modelling results. During December, the
7 measurements are most often larger than the model estimates. A similar observation can be
8 made at MON. Surprisingly, the measurements are significantly larger than the modelling
9 results, even when the wind blows from the North or North-East, i.e. when the Paris
10 agglomeration contribution is negligible (Dec 3rd, Dec 6-9, Dec 22-23). For these cases, the
11 most likely explanation is an underestimate of modelled CO₂ from the boundary conditions or
12 from emissions within the modelling domain outside of Île-de-France. Hereafter, we shall
13 denote this contribution as that from “remote fluxes”. Note that this impact from remote
14 fluxes shows a large increase of the mole fraction for the periods discussed above. We may
15 then hypothesize that this increase is underestimated. The interpretation is that anthropogenic
16 emissions from the Benelux area generate high concentrations that are underestimated in the
17 boundary condition field that is used in our simulations.

18 The EIF site is at the top of the Eiffel tower, 300 m above the Paris city. The wind speed for
19 this station is larger than for the other one, simply because it is higher in altitude. One expects
20 atmospheric mixing between the surface emissions and the inlet, so that the measurements are
21 representative of a larger area than e.g. MON and GON. Nevertheless there are some very
22 significant differences between the modelled and the observed mole fractions at EIF. The
23 differences may be huge, larger than 30 ppm, even during the afternoon, e.g on Oct 24th, Nov
24 7th, Dec 3rd, Dec 12th. Clearly, our atmospheric modelling framework cannot properly
25 represent the mole fraction time series at the EIF station, either because of strong local (sub
26 grid cell) emissions, or because of atmospheric transport processes that are not properly
27 represented, in particular concerning the vertical transport above the city. Further analysis of
28 the model-measurement mismatch is shown in [Figure S-3](#). The largest mismatches are
29 preferentially observed during the morning and for low wind speeds, but are observed at all
30 hours of the day and for all wind speed and directions, [which prevents from attributing these](#)
31 [mismatches to a specific bias in the transport model or to a bias in the estimate of the](#)
32 [emissions for a specific area.](#)

FMB 20/1/2015 18:45

Deleted: Figure S- 2.

FMB 20/1/2015 18:45

Deleted: .

1 The curves in Figure 5 and Figure S-1 show very large temporal variations of CO₂ within a
 2 day at all stations. Further analysis confirms that the largest variations are observed during
 3 the night, when the mixing layer is shallow. During the night and morning, the atmosphere is
 4 often very stable so that surface emissions accumulate within the lowest atmospheric layers,
 5 the thickness of which ranges from a few meters to tens of meters. The atmospheric mole
 6 fraction is then mostly sensitive to local fluxes and vertical mixing -an atmospheric process
 7 that is difficult to model- so that there is a large uncertainty about the [modelled](#) link between
 8 the emissions and the atmospheric mole fraction. [The](#) night-time and morning measurements
 9 are [thus](#) not appropriate for our flux inversion, as inverting them would be too sensitive to
 10 atmospheric transport biases. As a consequence, we focus on the concentration measurements
 11 acquired during the afternoon only, from noon to 4 p.m., when the mixing layer is usually
 12 well developed. [The](#) daily averages of these afternoon measured and modelled values are
 13 shown in Figure 5 as diamond symbols.

FMB 20/1/2015 18:45

Deleted: It is then clear that the

FMB 20/1/2015 18:45

Deleted: This justifies our choice of selecting only hourly measurements between noon and 4 p.m..

FMB 20/1/2015 18:45

Deleted: a large

14 2.6. Analyses and insight for the inverse modelling configuration

15 Both the measurements and the modelling results show [some](#) impact of the Paris area
 16 anthropogenic emissions on the CO₂ mole fractions at the 5 sites analysed here. The mole
 17 fraction increases over the modelled large-scale value depends on the wind speed and
 18 direction and a typical order of magnitude is 10 ppm. As expected, the signal is smaller for
 19 the rural station of TRN, which is further away from the city than the other sites. Many of the
 20 features in the measured time series are well reproduced by the modelling framework, which
 21 gives some confidence in its usefulness to improve the emission estimates.

22 There are also some significant differences between the measured and modelled mole
 23 fractions that cannot be justified by inaccurate emission inventories, [in the Paris area](#). The
 24 most obvious such feature is the mole fraction underestimate [at MON and GON](#) in northerly
 25 wind conditions when [these](#) sites are little sensitive to the Île-de-France emissions. This
 26 feature strongly suggests that remote fluxes lead to mole fraction increases that have biases
 27 with a typical magnitude that is similar to the impact of the Paris area emissions. [On the other](#)
 28 [hand](#), as the impact from remote fluxes is large scale, one may expect that this impact is
 29 similar for monitoring stations upwind and downwind from the Paris urban area. The [model-](#)
 30 [measurement](#) error may then be strongly reduced when analysing the difference [of mole](#)
 31 [fractions](#) between two stations [that are located upwind and downwind the Paris urban area](#),
 32 [respectively](#). On the other hand, the mole fraction difference between [such](#) stations [that are](#)

FMB 20/1/2015 18:45

Deleted: .

FMB 20/1/2015 18:45

Deleted: the MON and GON

FMB 20/1/2015 18:45

Deleted: These biases may have a significant impact on the flux inversion results.

FMB 20/1/2015 18:45

Deleted: boundary condition

FMB 20/1/2015 18:45

Deleted: mole fractions.

FMB 20/1/2015 18:45

Deleted: two

FMB 20/1/2015 18:45

Deleted: may

1 | close to the Paris area should contain a clear signature of the emissions from this area, and a
2 | relatively weak signature from other fluxes. It then suggests the use of downwind-upwind
3 | gradients in the CO₂ mole fractions rather than the absolute value of CO₂ measurements in the
4 | inversion procedure.

FMB 20/1/2015 18:45

Deleted: information on the Île-de-France emission when one lies upwind and the

FMB 20/1/2015 18:45

Deleted: downwind from the city

5 | The other significant feature in the comparison of the modelled and measured CO₂ mole
6 | fractions is much larger errors at the EIF site than at the other stations. These results illustrate
7 | the difficulty in modelling the CO₂ mole fraction within cities, even with a measurement inlet
8 | in altitude, well above the sources. Note that (McKain et al., 2012) also find very large (>30
9 | ppm) model-measurement mismatches within the urban area of Salt Lake City, even when
10 | using a high-resolution model. Similarly (Lac et al., 2013) finds large model-measurements
11 | differences at EIF despite the use of an urban parameterization in the modelling. The inability
12 | to properly model the CO₂ signal at EIF may have detrimental impact on the emission
13 | estimates derived from atmospheric inversion. Conversely, the forward simulations show that
14 | the TRN site is little sensitive to the Paris area emissions due to its location further away from
15 | the city than the other sites. Consequently, it cannot be used as a “downwind” site; in
16 | addition, GIF is better suited as an “upwind site” for southerly conditions as it is closer to the
17 | urban area and provides therefore a better information on the air composition as it enters the
18 | city. These features suggest not to use EIF and TRN and rather focus on MON, GON and
19 | GIF to estimate the Paris area emission from their measured mole fractions.

FMB 20/1/2015 18:45

Deleted: Clearly, the modelling of the atmospheric transport is inaccurate for this particular site. We put significant efforts to understand the origin of the large model-measurements mismatches at EIF (see supplementary Figure S- 2). Large modelling errors are observed for all wind directions.

FMB 20/1/2015 18:45

Deleted: a

20 | The main objective of the “gradient” inversion method is thus to focus on the monitoring
21 | stations that are at the edge of the urban area and to estimate the city scale emissions by
22 | removing most of the upwind signal from the measured and modelled concentrations. The
23 | upwind signal is driven by remote fluxes both from the boundary conditions and by fluxes
24 | within the model domain but outside the city whose estimates bear very large uncertainties.
25 | The inversion method also attempts to select the downwind measurements that are affected by
26 | the emissions from a large part of the city, in an attempt to minimize the impact of
27 | aggregation errors. Ideally, we would select only the wind direction when one station lies
28 | directly downwind from another, with the Paris city in between. However, given the very
29 | limited network of stations surrounding Paris, we have to broaden significantly the range of
30 | acceptable wind directions.

FMB 20/1/2015 18:45

Deleted: in

FMB 20/1/2015 18:45

Deleted: close vicinity

FMB 20/1/2015 18:45

Deleted: that are poorly modelled.

FMB 20/1/2015 18:45

Deleted: strongly

FMB 20/1/2015 18:45

Deleted: city

FMB 20/1/2015 18:45

Deleted: In the following, we therefore describe two attempts at inverting the Paris area emissions from the concentrations. The first one uses the 5 site records and relies on the boundary conditions provided by the large scale model. The second one only uses the measurements from GON, MON and GIF that are near-surface stations in the near vicinity of the Paris city, and the flux inversion

31 | Based on this analysis, the emission estimate procedure only uses the measurements from
32 | GON, MON and GIF and is based on the CO₂ mole fraction gradients between the upwind

1 and downwind stations, a method which requires the selection of favourable wind conditions.
2 The mathematical framework is described in the next section, while the inversion results are
3 presented in section 4.

4 3. Flux inversion

5 3.1. Principles

6 We follow a linear Bayesian inversion approach with Gaussian error statistics to determine
7 the optimal surface fluxes (anthropogenic emissions and biogenic fluxes) and their
8 uncertainties from a prior estimate of the fluxes and their uncertainties and from the mole
9 fraction measurements.

10 We call \mathbf{x} the state vector that gathers the scaling factors for the 6-hourly flux maps, \mathbf{x}_B its
11 prior estimate, \mathbf{H} the matrix operator that relates state parameters and mole fraction gradients
12 according to the atmospheric transport model, \mathbf{y} the observed mole fractions gradients, \mathbf{y}_F the
13 simulated impact on these mole fraction gradients of the lateral boundary conditions and of
14 the fluxes that are not accounted for in the state vector, \mathbf{B} the uncertainty covariance matrix of
15 \mathbf{x}_B , and \mathbf{R} the error covariance matrix of \mathbf{y} . These components are detailed in the next section.

16 The optimal solution is given by (Tarantola, 2005):

$$17 \quad \mathbf{x}_A = \mathbf{x}_B + (\mathbf{B}^{-1} + \mathbf{H}^T \mathbf{R}^{-1} \mathbf{H})^{-1} \mathbf{H}^T \mathbf{R}^{-1} (\mathbf{y} - \mathbf{y}_F - \mathbf{H} \mathbf{x}_B) \quad (1)$$

18 and its posterior error covariance matrix is

$$19 \quad \mathbf{A} = (\mathbf{B}^{-1} + \mathbf{H}^T \mathbf{R}^{-1} \mathbf{H})^{-1} \quad (2)$$

20 Note that \mathbf{A} does not depend on the actual measurement values, but varies, among other
21 factors, with their temporal and spatial sampling.

22 3.2. State vector: \mathbf{x}

23 Both the anthropogenic and biogenic prior fluxes described in Section 2 show a large diurnal
24 cycle that impacts the model simulations of CO_2 , and that is uncertain. It then appears useful
25 to invert this cycle together with the flux daily mean values. However, as discussed earlier,
26 only CO_2 measurements during the early afternoon can reliably be used to estimate the fluxes
27 and their information about the daily cycle is rather poor. We limit the number of
28 independent periods to 4 corresponding to the local times between 0-6 h, 6-12 h, 12-18 h, and
29 18-24 h, respectively.

FMB 20/1/2015 18:45

Deleted: very similar for these two inversions and is

FMB 20/1/2015 18:45

Deleted: . The results for

FMB 20/1/2015 18:45

Deleted: based on the 5 site measurements

FMB 20/1/2015 18:45

Deleted: discussed

FMB 20/1/2015 18:45

Deleted: 4; those for the inversion based on the gradients are in section 5.

FMB 20/1/2015 18:45

Deleted: variations

FMB 20/1/2015 18:45

Deleted: or mole fractions

FMB 20/1/2015 18:45

Deleted: fractions

FMB 20/1/2015 18:45

Formatted: Font:Bold

FMB 20/1/2015 18:45

Deleted: value

FMB 20/1/2015 18:45

Deleted: from CO_2 measurements

1 For the fossil fluxes, we use a scaling factor for each individual day in the state vector, which
 2 makes the number of corresponding variables amount to $30 \times 4 = 120$ for the 30-day period of
 3 the inversion. These scaling factors apply to the prior flux estimates derived from the AirParif
 4 inventory and are noted $\lambda_{0-6}^i, \lambda_{6-12}^i, \lambda_{12-18}^i, \lambda_{18-24}^i$ with i between 1 and 30.

5 Similarly, we optimize scaling factors of the prior NEE flux from C-TESSEL. The simulation
 6 domain shown in Figure 1 is split into 3×3 large boxes, and we choose the same 6-hour
 7 periods than for the anthropogenic fluxes to optimize scaling factors of NEE. However, we
 8 do not attempt a daily retrieval of NEE, and considered a single scaling factor for optimizing
 9 monthly NEE each 6-hour window over a 30-day inversion period. The number of variables
 10 to optimize NEE is therefore $3 \times 3 \times 4 = 36$. In the following, these NEE scaling factors are
 11 shown as $\alpha_{0-6}^X, \alpha_{6-12}^X, \alpha_{12-18}^X, \alpha_{18-24}^X$, where X is one of the 9 large boxes. One of the 9
 12 boxes covers the Île-de-France region, while the other ones are in the surrounding. In the
 13 *Inversion results* sections, we analyse the inversion of NEE for the centre box ($X=C$) together
 14 with those for the anthropogenic emissions. The surrounding boxes provide some ability to
 15 the inversion system to control part of the errors from remote NEE, but one cannot expect to
 16 get reliable estimate of the NEE in these areas given the weak observational constraint on this
 17 remote NEE.

18 The state vector \mathbf{x} for the linear inversion has therefore $120 + 36 = 156$ variables, that represent
 19 the scaling factors to the modelled fluxes. The prior value of each of these scaling factors in
 20 \mathbf{x}_B is 1.

3.3. Measurements gradients: \mathbf{y}

22 \mathbf{y} contains the measurements gradients that are used to constrain the flux inversion. As
 23 explained above, we only use hourly measurements that have been acquired during the
 24 afternoon from noon to 4 p.m. local time. In addition, the corresponding measurements need
 25 to have a sensitivity to local, unresolved, fluxes that is insignificant in comparison to that of
 26 larger scale fluxes. This condition is not met when the wind speed is low. We therefore use
 27 for the inversion only the measurements filtered for wind speeds larger than a given threshold
 28 at both sites used to compute the gradient. The results presented in this study are obtained
 29 with a threshold of 2 m s^{-1} . The wind speed estimate used for such a selection is the one
 30 analysed by the ECMWF at the location, height, and time of the observation. This criterion
 31 retains about 70% of the potential measurements.

FMB 20/1/2015 18:45

Deleted: independent

FMB 20/1/2015 18:45

Deleted: factors

FMB 20/1/2015 18:45

Deleted: for

FMB 20/1/2015 18:45

Deleted: so that we use

FMB 20/1/2015 18:45

Deleted: $\alpha_{0-6}^X, \lambda_{6-12}^X, \alpha_{12-18}^X, \alpha_{18-24}^X$

FMB 20/1/2015 18:45

Deleted: ,

FMB 20/1/2015 18:45

Deleted: degree of freedom

FMB 20/1/2015 18:45

Deleted: adjust

FMB 20/1/2015 18:45

Deleted: likely biased boundary conditions

FMB 20/1/2015 18:45

Deleted: Finally, there is one monthly variable (C_{offset}) in the state vector to adjust a possible large scale offset on the modelled concentrations over the domain and 30-day period.

FMB 20/1/2015 18:45

Deleted: $+1 = 157$

FMB 20/1/2015 18:45

Deleted: . The prior estimate for C_{offset} is 0 as the modelled is expected to reproduce the large-scale concentration with no bias, ... [2]

FMB 20/1/2015 18:45

Deleted: and have therefore a

FMB 20/1/2015 18:45

Deleted: 1.

FMB 20/1/2015 18:45

Deleted: the

FMB 20/1/2015 18:45

Deleted: be representative of a relativ ... [3]

FMB 20/1/2015 18:45

Deleted: that have been acquired with a

FMB 20/1/2015 18:45

Deleted: speed

FMB 20/1/2015 18:45

Deleted: . In the version of the inver ... [4]

FMB 20/1/2015 18:45

Deleted: here, the

FMB 20/1/2015 18:45

Deleted: is set at

FMB 20/1/2015 18:45

Deleted: is that

FMB 20/1/2015 18:45

Deleted: Note that the wind general ... [5]

In Equation (1) the [downwind-upwind differences in](#) mole fraction measurements y are corrected for the contributions that are not accounted for in the state vector (y_F). y_F are the modelled mole fraction accounting for the boundary conditions and anthropogenic fluxes outside Île-de-France (prescribed from the Edgar database). This contribution is shown as a blue line in Figure 5 and Figure S-1.

When the wind is from the South-West (upwind direction between 160° and 260°), GIF is considered as upwind from the [urban area](#), and the corresponding y elements are the differences between the mole fractions measured at either MON or GON and that measured at GIF. Similarly, when the wind is from the North-East (upwind direction between 0 and 135°), MON is used as an upwind reference to the GIF or GON mole fraction measurements. For other wind directions, the measurements are not assimilated.

3.4. Prior flux uncertainties and error correlations: B

Although we invert the scaling factors of fossil CO_2 emissions for each day and each 6-hour period, the uncertainties in these factors are correlated. We therefore attempt to assign correlations for the prior uncertainties based on several considerations: (i) the monthly budget for the AirParif inventory is generally stated to have an uncertainty of 20% which is used here; (ii) we assume small positive correlations between the different 6-hour windows; (iii) we assume stronger correlations from day to day for a given 6-hour window; (iv) the a priori uncertainty of individual 6-hour emission should have a typical order of 50%.

Based on these considerations, we set, rather arbitrarily, prior error correlations to 0.4 for two adjacent time periods (e.g. 12-18 and 18-24) and to 0.2 for non-adjacent time period (e.g. 6-12 and 18-24). For successive days, we use an exponential de-correlation with a characteristic time T_{cor} . The correlation between the prior uncertainties of the fossil CO_2 emissions scaling factors is then the product of this exponential and the [time-periods](#) correlation. For instance, the correlation between λ_{0-6}^5 and λ_{6-12}^9 is $0.4 \exp(-4/T_{cor})$. The results shown in this paper have been mostly obtained with a temporal correlation T_{cor} of 7 days, but other values, from 1 to 30 days, have been also tested. We have verified that such a **B** matrix is positive-definite. The desegregation of the assumed 20% uncertainty for the monthly emission totals, based on these temporal correlations, results in a standard deviation of uncertainties for individual 6-hour period of 33% ($T_{cor}=30$ days) to 50% ($T_{cor}=7$ days).

FMB 20/1/2015 18:45

Deleted: One version of the inversion system uses the measured mole fractions at the 5 sites. Following the discussion of Section 2.6, the other version is based on the gradients between the stations in the borders of the city area, i.e. GIF, MON and GON:

FMB 20/1/2015 18:45

Deleted: city

1 For the biogenic flux scaling factors, we set a relative prior uncertainty (standard deviation)
 2 close to 0.70 with some variations according to the box size (the variance varies inversely to
 3 the surface of the box), based on the numbers derived at 0.5° resolution in (Broquet et al.,
 4 2011). We do not assign any spatial / temporal correlation between the various biogenic
 5 scaling factors, i.e. between the 9 boxes or the 4 time periods. Similarly, there is no
 6 correlation in **B** between the prior uncertainties on the biogenic and anthropogenic fluxes.

7 3.5. Operator matrix: **H**

8 The operator matrix **H** provides the link between the surface fluxes and the mole fraction
 9 measurements. It combines the spatio-temporal distributions of the fluxes, both for the
 10 AirParif inventory and the C-Tessel biogenic fluxes, that are assumed and not modified
 11 through the inversion, the atmospheric transport by the Chimere model, the sampling of the
 12 atmosphere at the instrument locations and the selection of gradients according to the criteria
 13 developed in section 3.3. Note that the AirParif inventory has a 1 hour temporal resolution.
 14 The direct simulation (**H x**) uses the description of the emissions at this temporal resolution.
 15 Each element of the state vector corresponds to a natural or anthropogenic surface flux for a
 16 larger time period. We use the atmospheric transport model to compute the impact to the
 17 mole fraction of each surface flux (156 in total) corresponding to an element of the control
 18 vector. The 4D mole fraction fields from each of these simulations are then sampled at the
 19 place and time of the atmospheric observations, used to compute the downwind-upwind
 20 gradients corresponding to the observation vector. These simulated mole fraction gradients
 21 provides the elements of each column of the **H** matrix.

22 3.6. Observation error: **R**

23 The measurements provided by the instrument are precise, certainly better than 0.3 ppm.
 24 However, the observation error in **R** also includes any source of misfit between the model and
 25 the data that is not accounted for in the state vector such as the representation error, the
 26 impact of the error in the spatial distribution of the fluxes, and the atmospheric transport
 27 modelling error. These are difficult to assess (Broquet et al., 2013) although one expects
 28 significant values given the very heterogeneous urban environment that is discussed here.

29 Due to the complexity and misunderstanding of the processes underlying the observation
 30 error, that may lead to positive or negative correlations, we ignore observation error
 31 correlations in the construction of **R**, which is thus diagonal.

FMB 20/1/2015 18:45

Deleted: , neither between the offset mole fraction and the other parameters in the state vector. For C_{offset} , we assign an uncertainty of 5 ppm, corresponding to typical large-scale variations of the mole fractions at the boundary conditions

FMB 20/1/2015 18:45

Deleted: and

FMB 20/1/2015 18:45

Deleted: , except for C_{offset}

FMB 20/1/2015 18:45

Deleted: . This

FMB 20/1/2015 18:45

Deleted: For the *gradients* version of the inversion, the sampling is set as the difference between the simulated mole fractions at the two sites that are considered when the wind direction conditions described in section 3.3 are verified. By definition of this parameter, the column of the **H** matrix that corresponds to C_{offset} is set to 0 for the gradient version of the inversion, and 1 ppm for the other version. .

FMB 20/1/2015 18:45

Deleted: control

FMB 20/1/2015 18:45

Deleted: , both when assimilating individual mole fraction measurements and when assimilating mole fraction gradients

1 We use two statistical diagnostics of the misfits in the observation space described by
 2 (Desroziers et al., 2005) to infer typical observation error variances: (i) the agreement
 3 between the sum of the uncertainty from the prior estimate of the control parameters and of
 4 the observation error with the RMS of the prior misfits to the assimilated data; and (ii) the
 5 agreement between the observation error with the mean of the product of prior and posterior
 6 misfits to the assimilated data. Based on this analysis, we ~~set a 3~~ ppm observation error for
 7 the mole fraction gradients ~~that are used for the inversion~~.

8 We can note that this value is significantly smaller than the model-measurement differences
 9 as shown in Figure 5. This is due to the fact that the observation errors related to uncertainties
 10 in the large scale impact of the remote fluxes are strongly correlated between the
 11 measurement sites at a given time. Therefore, they vanish when considering gradients in the
 12 model fractions rather than values at individual sites such as in Figure 5. This is further
 13 discussed in section 4.2.

14 4. Inversion results

15 In the following, we present the result of the inversion described in the previous section. We
 16 first analyse the modelled mole fractions, prior and posterior, against the measurements. We
 17 then analyse the retrieved fluxes, both NEE and fossil fuel.

18 4.1. Mole fraction gradients

19 Figure 7 and Figure S4 show the time series of the afternoon-mean mole fraction gradients.
 20 Some days are missing either because either station is unavailable or because the wind
 21 direction does not fulfil the selection criteria developed in section 3.3. The prior value is
 22 almost always positive, because the reference is chosen upwind the Paris agglomeration.
 23 There are a few exceptions, like on Dec 22nd at GON, MON being used at the upwind
 24 reference according to the wind direction. As GON is in the northern part of the Paris
 25 agglomeration, one expects a smaller signal than for southerly wind conditions. Further
 26 investigation demonstrated that this unexpected behaviour is linked to a large spatial gradient
 27 of the CO₂ concentration generated by anthropogenic emissions over the Benelux accounted
 28 for in the Edgar inventory and transported by the Chimere model (y_f in equation 1).
 29 Interestingly, the observations confirm the sign and the order of magnitude of the gradient
 30 that is modelled with our setup that uses crude anthropogenic emissions outside Île-de-France.

FMB 20/1/2015 18:45
Deleted: infer
 FMB 20/1/2015 18:45
Deleted: 10
 FMB 20/1/2015 18:45
Deleted: EIF station and 5 ppm for the other sites when assimilating individual mole fraction measurements. When assimilating
 FMB 20/1/2015 18:45
Deleted: , we set a 3 ppm observation error
 FMB 20/1/2015 18:45
Deleted: We acknowledge that the two configurations are not consistent with each other. Indeed, if the observations errors were truly uncorrelated, as indicated by the use of a diagonal matrix for \mathbf{R} , the errors on the mole fraction gradients should be larger, by a ... [6]
 FMB 20/1/2015 18:45
Moved down [1]: Here, we have ... [7]
 FMB 20/1/2015 18:45
Moved down [2]: The Airparif inve ... [9]
 FMB 20/1/2015 18:45
Moved down [6]: This constitutes ... [17]
 FMB 20/1/2015 18:45
Moved down [7]: The second row ... [19]
 FMB 20/1/2015 18:45
Deleted: The theoretical posterior ... [10]
 FMB 20/1/2015 18:45
Moved down [3]: Most of the dai ... [11]
 FMB 20/1/2015 18:45
Moved down [4]: Note that the t ... [13]
 FMB 20/1/2015 18:45
Moved down [5]: These numbers ... [15]
 FMB 20/1/2015 18:45
Deleted: Although the inversion tool ... [8]
 FMB 20/1/2015 18:45
Deleted: The weekly cycle is appare ... [12]
 FMB 20/1/2015 18:45
Deleted: Conversely, the uncertainty ... [14]
 FMB 20/1/2015 18:45
Deleted: Of note is the peculiarity o ... [16]
 FMB 20/1/2015 18:45
Deleted: For the TRN tall tower sitc ... [18]
 FMB 20/1/2015 18:45
Deleted: variability. During the Oct ... [20]
 FMB 20/1/2015 18:45
Deleted: . On this particular date,
 FMB 20/1/2015 18:45
Deleted: chosen is MON
 FMB 20/1/2015 18:45
Moved (insertion) [8]
 FMB 20/1/2015 18:45
Deleted: The scatter plots of Figur ... [21]

1 Another negative gradient is observed at GIF-MON for northerly wind conditions, on Dec 3rd
2 This is very unexpected and we could not find a valid explanation for this particular case.
3 In general, the observations are smaller than the prior, and the posterior is in between.
4 Indeed, the inversion result leads to concentration gradient that are closer to the observations.
5 As a result, some of the posterior gradients are negative (see end of the period at GIF in
6 Figure 7).

7 Figure 8 and Figure S4 show scatter plots of measured versus modelled mole fractions
8 gradients. The first row of the plots on each of these figures shows the modelled mole
9 fractions from the domain boundaries and the fossil CO₂ emission outside Île-de-France
10 (black lines in Figure 5, y_F in equation 1) against the measurement. This constitutes the
11 modelled contribution to the mole fraction that is not optimized by the inversion. The values
12 on the Y-axis show the modelled impact of the remote fluxes on the upwind-downwind mole
13 fraction gradient. As expected, this impact is small compared to the measured gradient shown
14 on the X-axis.

15 The second row shows simulated CO₂ induced by prior NEE and fossil CO₂ fluxes (i.e. those
16 that are optimized through the inversion) against measured mole fractions corrected for the
17 large scale values (i.e. y_F , shown on the Y-axis of the first row). Although there is a large
18 spread, the correlation is significant, which shows that the transport model and the prior flux
19 set up have altogether some ability to reproduce the observed CO₂ mole fraction variability.
20 For the Oct-Nov period (in supplementary), the biases are large for all site gradients (2.1 to
21 4.8 ppm) whereas, for the Nov-Dec period, they are even larger at GIF-MON (7.1 ppm) but
22 rather small in comparison at both other sites. The standard deviation of the measurement-
23 model difference varies with the sites and period, between 2.0 and 5.8 ppm. This is
24 significantly smaller than the standard deviation for the mole fractions (Figures 6 and Figure
25 S2) that vary between 3.6 and 6.6 ppm. These smaller values confirm the choice made of
26 attempting an inversion based on the mole fraction gradient rather than the individual
27 observations.

28 After the inversion, the agreement is significantly improved as shown in the third row. Note
29 however that the standard deviation for the MON site (when GIF is used as a reference) is
30 slightly degraded from the prior value of 2.0 ppm. After the inversion, the correlation
31 between optimized and observed CO₂ gradients for all three stations is larger than 0.90. For
32 the other time period shown in the supplementary material (Figure S-5), the correlation

FMB 20/1/2015 18:45

Deleted: Although the modelling expects positive mole fraction gradients, the observed values can be

FMB 20/1/2015 18:45

Deleted: both

FMB 20/1/2015 18:45

Moved up [8]: As GON is in the northern part of the Paris agglomeration, one expects a smaller signal than for southerly wind conditions.

FMB 20/1/2015 18:45

Deleted: GON and

FMB 20/1/2015 18:45

Deleted: . At GON, negative values are found only in Northerly

FMB 20/1/2015 18:45

Deleted: , i.e. when MON is used as a reference.

FMB 20/1/2015 18:45

Deleted: The negative gradients values using GIF as a reference, in particular that of

FMB 20/1/2015 18:45

Deleted: are more surprisingly

FMB 20/1/2015 18:45

Deleted: them

FMB 20/1/2015 18:45

Deleted: As expected,

FMB 20/1/2015 18:45

Deleted: estimates of the mole fractions

FMB 20/1/2015 18:45

Deleted: than the prior. This is better shown

FMB 20/1/2015 18:45

Deleted: 10, which confirms that the statistics

FMB 20/1/2015 18:45

Moved (insertion) [6]

FMB 20/1/2015 18:45

Moved (insertion) [7]

FMB 20/1/2015 18:45

Deleted: have been

FMB 20/1/2015 18:45

Deleted: through

FMB 20/1/2015 18:45

Deleted: inversion.

FMB 20/1/2015 18:45

Deleted: (Figure S- 8),

statistics are not as good. However, this is due to a lower variability of the gradients, and the posterior standard deviations are 2.3, 2.7 and 2.3 ppm for the three sites, and are then similar as the values shown in Figure 7.

Overall, the statistics improve significantly between the prior and the posterior, and there is a good agreement between the measured and modelled mole fraction gradients. This raises confidence in our ability to model the impact of the Paris CO₂ emissions on the atmospheric concentrations for various wind conditions.

4.2. Daily flux estimates

Figure 9 shows the daily anthropogenic fluxes inferred by the inversion procedure. Here, we have aggregated the 4 6-hour periods as well as their uncertainty, accounting for the error correlations between the periods. Although the inversion controls scaling factors, we show here the resulting fluxes expressed in MtCO₂ per day. There is a clear weekly cycle on the prior emissions that are smaller during the week-ends. One may also note a shift in prior emission between Oct 29th and Nov 1st that corresponds to a change of month and therefore the switch to a different dataset in the AirParif inventory. The Airparif inventory includes a profile for October. For November and December, Airparif recommends the use of the January emission profile.

The uncertainty reduction is significant for all the days of the two time periods and a typical order of magnitude is a factor of 2. The emission uncertainty is reduced even for days with no usable measurements, when the wind direction is not within any of the two ranges defined in section 3.3, due to the temporal correlation of the uncertainties and thus of the corrections applied to the prior (section 3.4). The deviations of the flux estimate from the prior follow the gradient observation deviation from the model (see Figure 7). These deviations are mostly negative, although they are positive for a few days during both time periods. For the Nov-Dec period, the posterior emission estimates are within the bounds of the prior uncertainty range. On the other hand, the posterior estimate is much lower than the prior flux during the second half of the Oct-Nov period (Figure 9, top). Interestingly this period (Nov 1st to Nov 20st, 2010) was very mild [Meteo France, 2010] which suggests that the heating sector emissions were well below the AirParif inventory values for that period. During this season, according to the AirParif inventory, the heating sector, commercial and residential, amounts to more than 50% of the emission, so that the total emission is highly sensitive to temperature. Note that AirParif recommends the use of the January inventory for both November and

FMB 20/1/2015 18:45

Deleted: 10

FMB 20/1/2015 18:45

Deleted: The inverted daily fluxes based upon the gradient inversion are shown in Figure 11.

FMB 20/1/2015 18:45

Moved (insertion) [1]

FMB 20/1/2015 18:45

Moved (insertion) [2]

FMB 20/1/2015 18:45

Deleted: , like in the inversion of absolute mole fractions at each site.

FMB 20/1/2015 18:45

Deleted: 9

FMB 20/1/2015 18:45

Deleted: 11

December. As the temperatures are generally milder during October than January, one may expect that the inventory is larger than the true fluxes during October, which is then consistent with the negative correction to the fluxes during that period.

Figure 9 was generated using a 7 day correlation time for the emission uncertainties. We also tested similar inversions using different error correlation times (T_{cor}) in the range of the synoptic to seasonal time scales that drives the emission variability to assess the result sensitivity to this parameter. With a 1 day error correlation time, rather than 7 days used in our standard configuration, there are days with little or no flux constrain by the observations, while there is no smoothing of the day-to-day variability correction, resulting in an even larger spread of the retrieved fluxes (not shown). At the other extreme, a 30-day correlation time leads to much smoother results. Most of the daily-optimized flux estimates remain within the prior uncertainty range.

4.3. Monthly budgets

Figure 10 shows the monthly mean flux estimates for the Île-de-France region for the various 6-hour periods. It shows the results of the inversion for the anthropogenic emissions, the NEE of the central box that covers Ile de France, as well as the total. Note that the total estimate is necessarily the sum of the biogenic and anthropogenic fluxes. Conversely, the uncertainty range of the total is not a simple sum as it accounts for the correlations between NEE and fossil CO₂ emission errors in the A matrix linked to the difficulty in distinguishing NEE and fossil fluxes from the measurements.

The inversion has little impact on the fluxes for the 0-6h and 18-24h periods. On the other hand, the impact is strong for the 6-12h and 12-18h periods. This is because we only use afternoon observations that are sensitive to the emissions from the morning and afternoon periods only. The assigned correlations in the setup of the B matrix transport some constrain to the other time windows. Although the inversion based on the mole fraction gradients uses few independent observation, because of the additional data selection based on the wind direction, the impact on the flux estimates is significant.

Figure 10 shows that the uncertainty reduction is much larger for the fossil fuel than for the NEE. This is the result of the inversion based on the gradient downwind-upwind from the city which are mostly sensitive to the fluxes in between. The contribution from the NEE to the measurement is then small. Nevertheless, the correlations on the anthropogenic and NEE uncertainties are small (± 0.15 or less). These numbers indicate that the observation sampling

FMB 20/1/2015 18:45

Moved (insertion) [3]

FMB 20/1/2015 18:45

Deleted: 12

FMB 20/1/2015 18:45

Deleted: 30-day

FMB 20/1/2015 18:45

Deleted: , prior and posterior,

FMB 20/1/2015 18:45

Deleted: each one of

FMB 20/1/2015 18:45

Moved (insertion) [4]

FMB 20/1/2015 18:45

Deleted: As for the results shown in section 4, the

FMB 20/1/2015 18:45

Deleted: less

FMB 20/1/2015 18:45

Deleted: than the full inversion does

FMB 20/1/2015 18:45

Deleted: fewer sites and of an

FMB 20/1/2015 18:45

Deleted: of this setup

FMB 20/1/2015 18:45

Deleted: larger. One reason is

FMB 20/1/2015 18:45

Deleted: we have assigned lower

FMB 20/1/2015 18:45

Deleted: gradients

FMB 20/1/2015 18:45

Deleted: mole fractions as discussed in section 3.5. Another reason is that many measurements that are not used here, in particular those at TRN, but also those crosswind the Paris plume in the vicinity of the agglomeration, are little sensitive to the Île-de-France emissions so that they bring little information to the inversion when assimilating absolute mole fractions. Clearly, the setup

FMB 20/1/2015 18:45

Moved (insertion) [5]

provides significant information to distinguish NEE from fossil CO₂ fluxes in the inversion. Although a given measurement cannot trace the origin of the mole fraction excess, the assigned biogenic and anthropogenic flux errors have different spatial and temporal patterns which are exploited by the inversion system to attribute the mole fraction signal to specific sectors. However, this attribution relies on the a-priori spatial and temporal distribution of the fluxes that are affected by uncertainties. Thus, the theoretical ability of the system to disentangle natural and anthropogenic fluxes may not be realized in practice.

5. Discussion and Conclusions

This paper is a first attempt at estimating the Paris area emissions from measurements of atmospheric CO₂ mole fractions and prior flux knowledge. There is obviously room for improvement in several aspects of the inversion system: the number and spatial distribution of the monitoring stations, the atmospheric transport model including the use of an urban scheme, the [modelling](#) of concentration at the simulation domain boundaries, the definition of the emissions outside Île-de-France, the definition of the control vector, etc. However, first conclusions of broad implications beyond this first attempt can be drawn, that should guide further inverse modelling developments for Paris and other cities.

The analysis of the CO₂ time series shows significant differences between the measured and modelled mole fractions upwind the Paris city. These differences indicate that the simulated mole fraction at the domain boundaries may be off by several ppm. [The errors in this simulation is of similar magnitude as the signal from the Paris area emissions.](#) Although the number of cases is limited, it seems that the boundary concentrations are significantly underestimated when the wind is from the North or North-East (Benelux). These uncertainties on the domain boundaries generate large scale errors in the modelled mole fraction and suggest applying the inversion not on the measurements themselves, but rather on upwind-downwind gradients as was done in [this paper](#). Indeed, the measurement-model agreement is much better for the gradients [than it is for the direct values](#). It confirms that the large-scale pattern of CO₂ mole fraction, which is not related to the Île-de-France fluxes, is not properly modelled. The information provided by our five-site network does not allow optimizing the structure of the CO₂ boundary conditions, which is directly prescribed by a coarse scale global inversion. Exploiting the distant sites currently operational in Europe would unlikely improve this situation. In this context, the inversion based upon gradients as

FMB 20/1/2015 18:45

Deleted: retains the observations that do constrain the Paris agglomeration emissions, and should be recommended for future studies.

FMB 20/1/2015 18:45

Deleted: setting

FMB 20/1/2015 18:45

Deleted: section 5.

FMB 20/1/2015 18:45

Deleted: (Figure 10)

FMB 20/1/2015 18:45

Deleted: (Figure 8).

presented in section 4 appears necessary. It relies on the assumption that, due to atmospheric diffusion, the signature of remote fluxes upwind the city is sufficiently homogeneous in space, horizontally and vertically, and time over the path through the city from upwind to downwind sites both located within the afternoon PBL. As a consequence, the main part of such a large-scale signal is removed through the differences between two sites. The validity of this hypothesis is confirmed by the much better agreement between measured and modelled mole fractions as shown through the comparison of Figure 6 and Figure 8. Both measurements and atmospheric transport simulations indicate, however, that the CO₂ mole fraction signal generated by distant sources outside the Chimere model domain has some spatial structures (see e.g. the variability of modelled values in Figure 10). As a consequence, distant sources and sink do impact the inversion, even when using the concentration gradients, although the resulting biases on the retrieved fluxes are very much reduced compare to the inversion setup of sect. ... [22]

FMB 20/1/2015 18:45

Deleted: 5 appears more reliable than those of section 4 so that this setup should be our baseline for future improvements. However, both measurements and atmospheric transport simulations indicate that the CO₂ mole fraction signal generated by distant sources outside the Chimere model domain has some spatial structures (see e.g. the variability of modelled values in Figure 10). As a consequence, distant sources and sink do impact the inversion, even when using the concentration gradients, although the resulting biases on the retrieved fluxes are very much reduced compare to the inversion setup of sect. ... [22]

FMB 20/1/2015 18:45

Deleted: Figure 8 and Figure 10.

The drawback of using the gradient-based inversion method is a reduction in the number of observations, in particular with the current monitoring network that only samples a fraction of possible wind directions. Nevertheless, although the number of observations is very much reduced, our inversion system based on the gradient reports significant uncertainty reductions. It must also be noted that we assumed a 7-day error correlation time for the anthropogenic emissions, so that our system shows flux uncertainty reductions, even on days with no valid observation as the flux is constrained by observation of the previous or following days.

FMB 20/1/2015 18:45

Deleted: The smaller observation error on the gradients, compared to the absolute mole fractions, allows assigning smaller values in the **R** vector, which leads to a larger constraint by the available observations.

FMB 20/1/2015 18:45

Deleted: length

The setting of temporal error correlation on prior fluxes is therefore essential for the inversion. Although the results in this paper are mostly derived with a 7-day correlation length, this is a somewhat arbitrary choice, and the results are significantly affected when using different values. In particular, a much shorter value (1 day) leads to very large variations in the posterior daily emissions. Further work should be devoted to the assignment of objective correlation lengths based on the processes that lead to emission uncertainties. Climatic conditions in general, and more specifically temperature during the cold season, influence the emission with a time scale that is consistent with synoptic events, i.e. close to a week; the impact of specific events such as holidays, commemorations or strikes have a much shorter time scale, while inventory biases linked to e.g. the emission factors have an impact on the fluxes on time scales of months or even larger.

FMB 20/1/2015 18:45

Deleted: For such short correlation length, the days with no valid observations show a posterior emission that is close to the prior value whereas the flux change, from prior to posterior, is large for the days with observations.

FMB 20/1/2015 18:45

Deleted: The atmospheric temperature

Our analysis also indicates model-measurement discrepancies at the EIF site, that are much larger than at other sites. On the one hand, this is somewhat surprising as measurement inlet

FMB 20/1/2015 18:45

Deleted: , i.e. at the top of the Eiffel tower,

1 in altitude should insure a larger spatial representativeness than at the surface sites and less
2 sensitivity to local, poorly represented, emissions. Usually, tall tower-based measurements
3 are preferred to those at the surface for the estimate of biogenic fluxes. On the other hand,
4 EIF is located close to the centre of the Paris city and is therefore affected by stronger local
5 emissions than the other sites used in this paper. City fluxes are highly heterogeneous while
6 the model used in this paper has a 2 km spatial resolution, does not include information on the
7 3D structure of the urban canopy, and uses limited information on the CO₂ source injection
8 heights. Such model may then be insufficient to properly account for atmospheric processes
9 that link the [local](#) surface fluxes to the concentrations at the top of the Eiffel tower. Previous
10 results obtained at MeteoFrance by (Lac et al., 2013) using a high (2 km) resolution
11 meteorological model that includes urban parameterizations, and validated against local
12 meteorological measurements, also show high model-data misfits at EIF, similar to those
13 found in the present paper. (McKain et al., 2012) also show a poor skill at representing the
14 mole fraction at urban sites, so that the information content of the measurements is not
15 applied for an estimate of the absolute emissions, but rather for a on long term relative
16 change. These [findings can be related to](#) our difficulties for modelling urban CO₂ at EIF using
17 a 2 km resolution transport model are typical of the current generation of models. The use of
18 urban sites such as EIF for atmospheric inversion will likely necessitate long term research by
19 the inverse modelling and transport modelling communities.

20

21 At present, our mesoscale atmospheric transport model cannot reconcile the measurements at
22 the top of the tower with those at the surface in the vicinity of the city, given our set of
23 surface fluxes and inversion settings. [This](#) cast doubts on the quality of the modelling at the
24 other sites. Indeed, if the atmospheric transport model does not properly simulate the
25 atmospheric vertical transport between the surface and an inlet at 300 m in altitude, it likely
26 misrepresents the link between surface fluxes and atmospheric mole fractions. Conversely,
27 the large modelling errors at EIF may be related to its urban location (and to the strong
28 influence of local urban sources) and this would raise concerns regarding the ability to exploit
29 urban measurements, and therefore to solve for the spatial distribution of the fluxes within the
30 urban area.

31

FMB 20/1/2015 18:45

Deleted: studies confirm that

FMB 20/1/2015 18:45

Deleted: Our solution has been to disregard the measurements from the EIF site in a best attempt at inverting the Île-de-France CO₂ fluxes. However, our inability to reproduce the EIF mole fraction measurements

1 The largest differences between the measured and modelled concentrations occur for low
 2 wind speeds. For this reason, we have chosen a 2 m s^{-1} wind speed threshold below which the
 3 measurements are not used in the inversion. A larger threshold rejects further observations,
 4 and reduces the range of ~~flux corrections through the inversion~~. The choice of the threshold is
 5 ~~somewhat~~ arbitrary and we have refrained from using a large one to clearly demonstrate the
 6 impact of a few situations with low wind-speed. There are several hypotheses for the poor
 7 modelling at low wind speed, including larger representativity errors of subgrid patterns, or
 8 larger errors in vertical mixing modelling. However, such issues are continuous and there is
 9 no indication that the modelling errors disappear between e.g. 2 and 3 m s^{-1} . Thus, further
 10 rejection of low wind-speed observations may hide the deficiencies in the atmospheric
 11 transport without improving the flux inversion.

12

13 We also stress that our analysis is based on measurements during the late fall period. This is a
 14 favourable case for the inversion of fossil fuel CO_2 emissions as there is less interference with
 15 the biogenic fluxes (Pataki et al., 2007). During spring and summer, the NEE is much larger
 16 (in absolute value) and also more uncertain. In fact, during May, the biogenic sink is likely
 17 larger than the anthropogenic emissions within Île-de-France as shown by [Figure 3 and Figure](#)
 18 [S4. The gradient inversion method](#) is designed to also minimize this interference of biogenic
 19 flux with the constraint on anthropogenic fluxes. Indeed, the theoretical posterior
 20 uncertainties indicate little correlations between the retrieved NEE and anthropogenic
 21 emissions. ~~There is however vegetation within the urban area that may generate a significant~~
 22 ~~sink during the growing season~~. A successful anthropogenic emission inversion ~~would~~
 23 ~~benefit from additional~~ efforts for describing the biogenic fluxes and the use of additional
 24 tracers such as ^{14}C to ~~separate the signature of~~ fossil fluxes and biogenic emissions. One
 25 future direction is thus to use a more realistic NEE model over the Paris area, that could be
 26 calibrated upon local eddy covariance observations (e.g. the method used in (Gerbig et al.,
 27 2003)) and satellite land cover and vegetation activity.

28

29 The prior estimate of the Île-de-France CO_2 emissions does not account for the human
 30 respiration. Yet, within dense urban areas, human respiration can be a significant fraction of
 31 the fossil fuel emissions (Ciais et al., 2007) (Widory and Javoy, 2003). Respiration by human
 32 ~~beings~~ is a source of CO_2 of typically $1 \text{ kgCO}_2 \text{ day}^{-1}$ (Prairie and Duarte, 2007) which,

FMB 20/1/2015 18:45

Deleted: inverted daily fluxes.

FMB 20/1/2015 18:45

Deleted: clearly

FMB 20/1/2015 18:45

Deleted: Figure 3 and Figure 4. Individual mole fraction measurements cannot distinguish the origin of the concentration signal while the uncertainties on the biogenic fluxes are larger than those on the anthropogenic fluxes. The gradient inversion set-up

FMB 20/1/2015 18:45

Deleted: However, these results are based on strong assumptions in particular that the spatial and temporal distributions of the NEE fluxes are known

FMB 20/1/2015 18:45

Deleted: large areas. Therefore, in the real world, the inversion

FMB 20/1/2015 18:45

Deleted: still attribute some flux changes that are necessary to fit the concentrations to the biogenic rather than anthropogenic fluxes. It is certainly possible to estimate independently the biogenic and fossil fluxes from

FMB 20/1/2015 18:45

Deleted: large set of measurements but a successful inversion relies on an accurate description of the spatial and temporal distribution of both.

FMB 20/1/2015 18:45

Deleted: still requires significant

FMB 20/1/2015 18:45

Deleted: distinguish

1 assuming a total population of 11.7 millions for the Île-de-France, leads to 4.2 MtCO₂ per
2 year, or 8% of the AirParif fossil fuel inventory. Although small, this [flux](#) is far from
3 negligible, [compared to fossil fuel emissions](#). While the CO₂ mole fraction measurements are
4 sensitive to the human respiration flux, our control vector only accounts for the fossil fuel
5 emissions and NEE fluxes. Although [it does not have point sources](#), the spatial distribution of
6 the human respiration is [broadly](#) similar to that of the fossil fuel emissions, so that the
7 inversion will attribute the human respiration mole fraction signal to the fossil fuel rather than
8 the NEE fluxes. We therefore expect an overestimate of the fossil fuel emission by typically
9 [8% in our inversion that neglects human respiration](#). A larger percentage may be expected in
10 summer and a smaller in winter due to the seasonal cycle of the fossil fuel emissions that has
11 a larger relative amplitude than that of the human respiration. Improvement of our inversion
12 system should explicitly account for the human respiration, based on the spatial distribution of
13 the population.

14

15 One often stated objective of the top-down inversion of fossil fuel CO₂ emissions is to
16 provide an independent verification of the bottom-up estimates, i.e. the inventories (Levin et
17 al., 2011; McKain et al., 2012; Duren and Miller, 2012). However, information about the
18 spatial and temporal distribution of the emissions has to be used for inverse modelling to limit
19 aggregation errors on the overall budget. In our case, the number of monitoring stations is far
20 too small to independently invert the spatial distribution of the emissions. We have been able
21 to rely on the comprehensive distribution from AirParif. With a larger number of monitoring
22 stations, it may be possible to estimate some information about the flux spatial distribution,
23 but atmospheric transport is not a reversible process and some accurate information about the
24 spatial distribution will likely be needed, so that the atmospheric inversion cannot be seen as
25 independent from the inventories, but rather as a mean to verify or refine them. In addition,
26 as long as the accuracy on the atmospheric transport makes does not allow using night-time or
27 morning measurements, it will not be possible to monitor the daily cycle of the emissions.
28 Thus, the computation of daily or monthly fluxes requires some robust information about the
29 daily cycle that should rely on inventories. Thus, again, our top-down emission estimate is far
30 from independent from the bottom-up inventory.

31

FMB 20/1/2015 18:45

Deleted: number

FMB 20/1/2015 18:45

Deleted: .

FMB 20/1/2015 18:45

Deleted: different

FMB 20/1/2015 18:45

Deleted: %.

1 Although the inversion procedure provides a posterior uncertainty estimate, one should
2 ~~interpret this~~ uncertainty with caution. Indeed, the mathematical framework used here relies
3 on a number of hypotheses, some of which are crude approximations of the reality, such as
4 the spatial and temporal correlations in the flux uncertainties or the unbiased atmospheric
5 transport modelling. The impact of these assumptions has not been quantified. Although we
6 have no “truth” to benchmark ~~the inversion results~~, and there are not even enough
7 measurement sites to perform ‘leave-one-out’ tests, one can perform some sanity checks on
8 the results. One sanity check is the comparison of the measured and modelled mole fractions
9 (Figure 8 and Figure ~~S4~~). The analysis of these figures confirms the ability of our inversion
10 ~~to improve the measurement-model agreement~~. Nevertheless, we note that the posterior
11 misfit (≈ 2.5 ppm) is still a significant fraction of the signal that is analysed (10-20 ppm). The
12 crucial question is whether the atmospheric modelling error is random or a bias and we have
13 no element to answer that question. The other sanity check consists in analysing the validity
14 of the retrieved daily fluxes (Figure 9). In this respect, the daily fluxes show day-to-day
15 variations that are suspicious, although not refutable at this stage. A result that points in
16 favour of the flux inversions shown here is the significant reduction from the prior during a
17 period with temperatures above the seasonal normal, and the negative correction of the
18 emissions during November from the prior value that is based on an inventory simulating
19 January emissions. A single such event is certainly not sufficient to validate the inversion
20 system, however. We shall apply the same inversion setup to more than a year of
21 measurements and analyse the results with respect to the temperature anomaly or other short-
22 term event that may have a significant influence on the Île-de-France CO₂ emissions. More
23 measurement sites are needed to better evaluate the skill of the inversion. The deployment of
24 a network of 5 sites around Paris within the framework of the CarboCount-City project will
25 help in this direction. ~~In addition, inlet at different altitudes will be installed on the Eiffel~~
26 ~~tower station for a better assessment of the CO₂ vertical distribution and transport within the~~
27 ~~urban area. These will be most useful for the longer-term objective of improving the~~
28 ~~atmospheric transport modelling within the city, which may allow the EIF measurements to~~
29 be used ~~by~~ the inversion system. ▽

FMB 20/1/2015 18:45

Formatted: Justified

FMB 20/1/2015 18:45

Deleted: use such

FMB 20/1/2015 18:45

Deleted: our

FMB 20/1/2015 18:45

Deleted: 10

FMB 20/1/2015 18:45

Deleted: set-up to

FMB 20/1/2015 18:45

Deleted: the concentration gradients much better than the individual absolute measurements

FMB 20/1/2015 18:45

Deleted: 11

FMB 20/1/2015 18:45

Deleted: A

FMB 20/1/2015 18:45

Deleted: task consists in

FMB 20/1/2015 18:45

Deleted: so that the measurement from the Eiffel tower top can

FMB 20/1/2015 18:45

Deleted: in

FMB 20/1/2015 18:45

Deleted: .

Acknowledgments

This study was conducted within the ANR CO2-Megaparis project and was made possible thanks to funding from the CarboCount and CarboCount-city projects that are co-funded by the Climate KIC program of the European Institute of Technology. [Gregoire Broquet acknowledges funding and support from the Chaire industrielle BridGES, a joint research program between Thales Alenia Space, Veolia, Université de Versailles Saint Quentin en Yvelines, CEA and CNRS.](#) We thank Lin Wu and Isabelle Pison for assistance as well as all the developers of the AirParif inventory.

References

- Boussetta, S., Balsamo, G., Beljaars, A., Panareda, A. A., Calvet, J. C., Jacobs, C., van den Hurk, B., Viterbo, P., Lafont, S., Dutra, E., Jarlan, L., Balzarolo, M., Papale, D., and van der Werf, G.: Natural land carbon dioxide exchanges in the ECMWF integrated forecasting system: Implementation and offline validation, *J Geophys Res-Atmos*, 118, 5923-5946, Doi 10.1002/Jgrd.50488, 2013.
- Broquet, G., Chevallier, F., Rayner, P., Aulagnier, C., Pison, I., Ramonet, M., Schmidt, M., Vermeulen, A. T., and Ciais, P.: A European summertime CO2 biogenic flux inversion at mesoscale from continuous in situ mixing ratio measurements, *J Geophys Res-Atmos*, 116, Artn D23303, doi 10.1029/2011jd016202, 2011.
- Broquet, G., Chevallier, F., Breon, F. M., Kadygrov, N., Alemanno, M., Apadula, F., Hammer, S., Haszpra, L., Meinhardt, F., Morgui, J. A., Necki, J., Piacentino, S., Ramonet, M., Schmidt, M., Thompson, R. L., Vermeulen, A. T., Yver, C., and Ciais, P.: Regional inversion of CO2 ecosystem fluxes from atmospheric measurements: reliability of the uncertainty estimates, *Atmos Chem Phys*, 13, 9039-9056, Doi 10.5194/Acp-13-9039-2013, 2013.
- Chevallier, F., Ciais, P., Conway, T. J., Aalto, T., Anderson, B. E., Bousquet, P., Brunke, E. G., Ciattaglia, L., Esaki, Y., Frohlich, M., Gomez, A., Gomez-Pelaez, A. J., Haszpra, L., Krummel, P. B., Langenfelds, R. L., Leuenberger, M., Machida, T., Maignan, F., Matsueda, H., Morgui, J. A., Mukai, H., Nakazawa, T., Peylin, P., Ramonet, M., Rivier, L., Sawa, Y., Schmidt, M., Steele, L. P., Vay, S. A., Vermeulen, A. T., Wofsy, S., and Worthy, D.: CO2 surface fluxes at grid point scale estimated from a global 21 year reanalysis of atmospheric measurements, *J Geophys Res-Atmos*, 115, Artn D21307, doi 10.1029/2010jd013887, 2010.
- Ciais, P., Bousquet, P., Freibauer, A., and Naegler, T.: Horizontal displacement of carbon associated with agriculture and its impacts on atmospheric CO2, *Global Biogeochem Cy*, 21, Artn Gb2014, doi 10.1029/2006gb002741, 2007.
- Desroziers, G., Berre, L., Chapnik, B., and Poli, P.: Diagnosis of observation, background and analysis-error statistics in observation space, *Q J Roy Meteor Soc*, 131, 3385-3396, Doi 10.1256/Qj.05.108, 2005.
- Duren, R. M., and Miller, C. E.: COMMENTARY: Measuring the carbon emissions of megacities, *Nat Clim Change*, 2, 560-562, 2012.

FMB 20/1/2015 18:45

Deleted: KIC

FMB 20/1/2015 18:45

Deleted: Doi 10.1029/2011jd016202, 2011. -

FMB 20/1/2015 18:45

Deleted: -

... [23]

FMB 20/1/2015 18:45

Deleted: -

... [24]

1 Gerbig, C., Lin, J. C., Wofsy, S. C., Daube, B. C., Andrews, A. E., Stephens, B. B., Bakwin,
2 P. S., and Grainger, C. A.: Toward constraining regional-scale fluxes of CO₂ with
3 atmospheric observations over a continent: 1. Observed spatial variability from airborne
4 platforms, *J Geophys Res-Atmos*, 108, Artn 4756, doi 10.1029/2002jd003018, 2003.

5 Gurney, K. R., Law, R. M., Denning, A. S., Rayner, P. J., Baker, D., Bousquet, P., Bruhwiler,
6 L., Chen, Y. H., Ciais, P., Fan, S., Fung, I. Y., Gloor, M., Heimann, M., Higuchi, K., John, J.,
7 Maki, T., Maksyutov, S., Masarie, K., Peylin, P., Prather, M., Pak, B. C., Randerson, J.,
8 Sarmiento, J., Taguchi, S., Takahashi, T., and Yuen, C. W.: Towards robust regional
9 estimates of CO₂ sources and sinks using atmospheric transport models, *Nature*, 415, 626-
10 630, Doi 10.1038/415626a, 2002.

11 Gurney, K. R., Razlivanov, I., Song, Y., Zhou, Y. Y., Benes, B., and Abdul-Massih, M.:
12 Quantification of Fossil Fuel CO₂ Emissions on the Building/Street Scale for a Large US
13 City, *Environ Sci Technol*, 46, 12194-12202, Doi 10.1021/Es3011282, 2012.

14 Kort, E. A., Frankenberg, C., Miller, C. E., and Oda, T.: Space-based observations of
15 megacity carbon dioxide, *Geophys Res Lett*, 39, Artn L17806, doi 10.1029/2012gl052738,
16 2012.

17 Lac, C., Donnelly, R. P., Masson, V., Pal, S., Riette, S., Donier, S., Queguiner, S., Tanguy,
18 G., Ammoura, L., and Xueref-Remy, I.: CO₂ dispersion modelling over Paris region within
19 the CO₂-MEGAPARIS project, *Atmos Chem Phys*, 13, 4941-4961, Doi 10.5194/Acp-13-
20 4941-2013, 2013.

21 Lauvaux, T., Pannekoucke, O., Sarrat, C., Chevallier, F., Ciais, P., Noilhan, J., and Rayner, P.
22 J.: Structure of the transport uncertainty in mesoscale inversions of CO₂ sources and sinks
23 using ensemble model simulations, *Biogeosciences*, 6, 1089-1102, 2009.

24 Lauvaux, T., Schuh, A. E., Uliasz, M., Richardson, S., Miles, N., Andrews, A. E., Sweeney,
25 C., Diaz, L. I., Martins, D., Shepson, P. B., and Davis, K. J.: Constraining the CO₂ budget of
26 the corn belt: exploring uncertainties from the assumptions in a mesoscale inverse system,
27 *Atmos Chem Phys*, 12, 337-354, Doi 10.5194/Acp-12-337-2012, 2012.

28 Levin, I., Hammer, S., Eichmann, E., and Vogel, F. R.: Verification of greenhouse gas
29 emission reductions: the prospect of atmospheric monitoring in polluted areas, *Philosophical*
30 *transactions. Series A, Mathematical, physical, and engineering sciences*, 369, 1906-1924,
31 10.1098/rsta.2010.0249, 2011.

32 Lopez, M., Schmidt, M., Delmotte, M., Colomb, A., Gros, V., Janssen, C., Lehman, S. J.,
33 Mondelain, D., Perrussel, O., Ramonet, M., Xueref-Remy, I., and Bousquet, P.: CO, NO_x and
34 (CO₂)-C-13 as tracers for fossil fuel CO₂: results from a pilot study in Paris during winter
35 2010, *Atmos Chem Phys*, 13, 7343-7358, Doi 10.5194/Acp-13-7343-2013, 2013.

36 McKain, K., Wofsy, S. C., Nehrkorn, T., Eluszkiewicz, J., Ehleringer, J. R., and Stephens, B.
37 B.: Assessment of ground-based atmospheric observations for verification of greenhouse gas
38 emissions from an urban region, *P Natl Acad Sci USA*, 109, 8423-8428, Doi
39 10.1073/Pnas.1116645109, 2012.

40 Menut, L., Bessagnet, B., Khvorostyanov, D., Beekmann, M., Blond, N., Colette, A., Coll, I.,
41 Curci, G., Foret, G., Hodzic, A., Mailler, S., Meleux, F., Monge, J. L., Pison, I., Siour, G.,
42 Turquety, S., Valari, M., Vautard, R., and Vivanco, M. G.: CHIMERE 2013: a model for
43 regional atmospheric composition modelling, *Geosci Model Dev*, 6, 981-1028, Doi
44 10.5194/Gmd-6-981-2013, 2013.

FMB 20/1/2015 18:45

Deleted: Doi 10.1029/2002jd003018, 2003. .

FMB 20/1/2015 18:45

Deleted: .

... [25]

1 Nehrkorn, T., Henderson, J., Leidner, M., Mountain, M., Eluszkiewicz, J., McKain, K., and
2 Wofsy, S.: WRF Simulations of the Urban Circulation in the Salt Lake City Area for CO₂
3 Modeling, *J Appl Meteorol Clim*, 52, 323-340, Doi 10.1175/Jamc-D-12-061.1, 2013.

4 Nordbo, A., Jarvi, L., Haapanala, S., Wood, C. R., and Vesala, T.: Fraction of natural area as
5 main predictor of net CO₂ emissions from cities, *Geophys Res Lett*, 39, Artn L20802, doi
6 [10.1029/2012gl053087](https://doi.org/10.1029/2012gl053087), 2012.

7 [Pal, S., Xueref-Remy, I., Ammoura, L., Chazette, P., Gibert, F., Royer, P., Dieudonne, E.,](#)
8 [Dupont, J. C., Haeffelin, M., Lac, C., Lopez, M., Morille, Y., and Ravetta, F.: Spatio-temporal](#)
9 [variability of the atmospheric boundary layer depth over the Paris agglomeration: An](#)
10 [assessment of the impact of the urban heat island intensity, *Atmos Environ*, 63, 261-275, Doi](#)
11 [10.1016/J.Atmosenv.2012.09.046](#), 2012.

12 Pataki, D. E., Alig, R. J., Fung, A. S., Golubiewski, N. E., Kennedy, C. A., McPherson, E. G.,
13 Nowak, D. J., Pouyat, R. V., and Lankao, P. R.: Urban ecosystems and the North American
14 carbon cycle, *Global Change Biol*, 12, 2092-2102, Doi 10.1111/J.1365-2486.2006.01242.X,
15 2006.

16 Pataki, D. E., Xu, T., Luo, Y. Q., and Ehleringer, J. R.: Inferring biogenic and anthropogenic
17 carbon dioxide sources across an urban to rural gradient, *Oecologia*, 152, 307-322, Doi
18 10.1007/S00442-006-0656-0, 2007.

19 Peylin, P., Rayner, P. J., Bousquet, P., Carouge, C., Hourdin, F., Heinrich, P., Ciais, P., and
20 Contributors, A.: Daily CO₂ flux estimates over Europe from continuous atmospheric
21 measurements: 1, inverse methodology, *Atmos Chem Phys*, 5, 3173-3186, 2005.

22 Prairie, Y. T., and Duarte, C. M.: Direct and indirect metabolic CO₂ release by humanity,
23 *Biogeosciences*, 4, 215-217, 2007.

24 Shepson, P. B., Cambaliza, M., Davis, K., Gurney, K., Lauvaux, T., Richardson, N.,
25 Richardson, S., Sweeney, C., and Turnbull, J.: Indianapolis flux experiment (INFLUX):
26 Experiment design and new results regarding measurements of urban-area CO₂ and CH₄
27 emission fluxes, *Abstr Pap Am Chem S*, 242, 2011.

28 Tarantola, A.: Inverse problem theory and methods for model parameter estimation, Society
29 for Industrial and Applied Mathematics, Philadelphia, PA, xii, 342 p. pp., 2005.

30 Widory, D., and Javoy, M.: The carbon isotope composition of atmospheric CO₂ in Paris,
31 *Earth Planet Sc Lett*, 215, 289-298, Doi 10.1016/S0012-821x(03)00397-2, 2003.

32 Zhao, C. L., and Tans, P. P.: Estimating uncertainty of the WMO mole fraction scale for
33 carbon dioxide in air, *J Geophys Res-Atmos*, 111, Artn D08s09, doi [10.1029/2005jd006003](https://doi.org/10.1029/2005jd006003),
34 [2006](#).

FMB 20/1/2015 18:45

Deleted: Doi 10.1029/2012gl053087, 2012. .

FMB 20/1/2015 18:45

Deleted: Doi 10.1029/2005jd006003, 2006. .

1 **Tables and captions**

2

3 Table 1 : Information about the CO₂ measuring stations that are used in this paper.

4

Location	Acronym	Latitude [°]	Longitude [°]	Height AGL [m]	Distance from Paris centre [km]
Eiffel Tower	EIF	48.8582	2.2946	300	4 (W)
Montgé-en-Goële	MON	49.0284	2.7489	9	35 (NE)
Gonesse	GON	48.9908	2.4446	4	16 (N)
Gif sur Yvette	GIF	48.7100	2.1475	7	23 (SW)
Trainou Forest	TRN	47.9647	2.1125	180	101 (S)

5

6

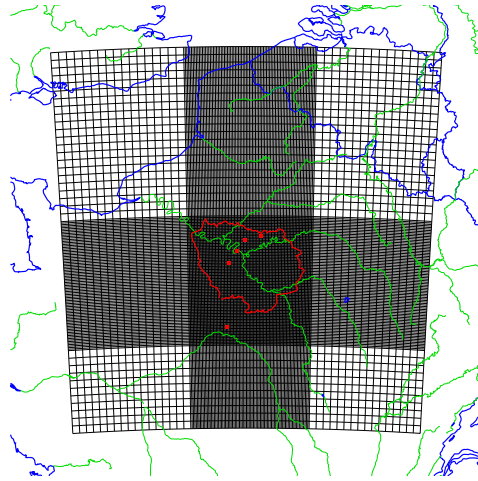


Figure 1 : Map of the study area showing the location of the continuous CO₂ measurement stations that are used in this paper (red dots). The black lines show the model grid with a 2 km resolution at the centre, and 10 km on the sides. The red line shows the limits of the Île-de-France region.

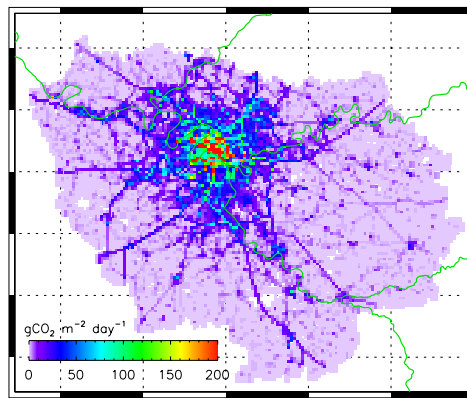


Figure 2 : Typical day-total CO₂ emissions of Île-de-France, according to AirParif year 2008 inventory, for a weekday in October. The point sources are not included in this map. The emissions are provided for the area outlined in red in Figure 1. The resolution is 1 km. The grid is 0.2° in latitude and 0.4° in longitude.

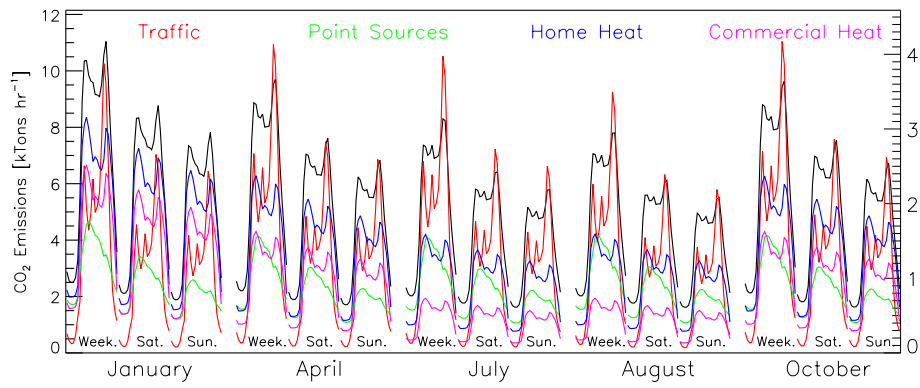


Figure 3: Temporal variation of the main CO₂ emission sectors according to the AirParif inventory for the whole Ile de France region. The figure shows, for 5 typical months and 3 typical days (Weekday, Saturday, Sunday), the hourly CO₂ emissions. The black line is the total emission (left scale) while the four coloured lines are for different sectors (right scale).

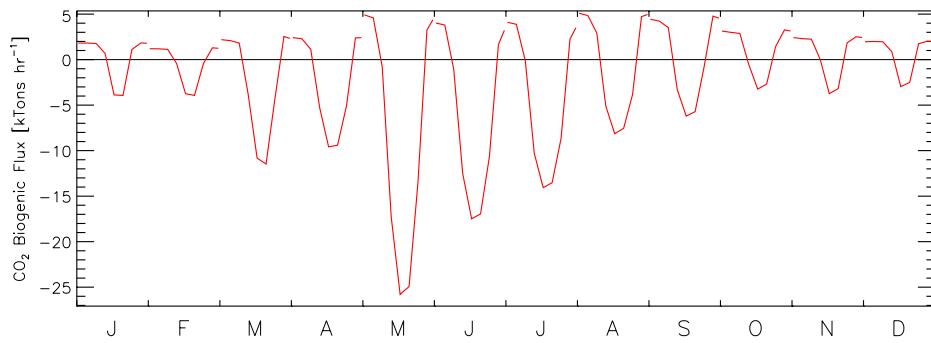


Figure 4: Mean diurnal cycle of the biogenic flux (Net Ecosystem exchange) for the 12 calendar months and for the same area as in Figures 2 and 3 which is outlined in red in Figure 1. The values were derived from an average of the C-Tessel simulations.

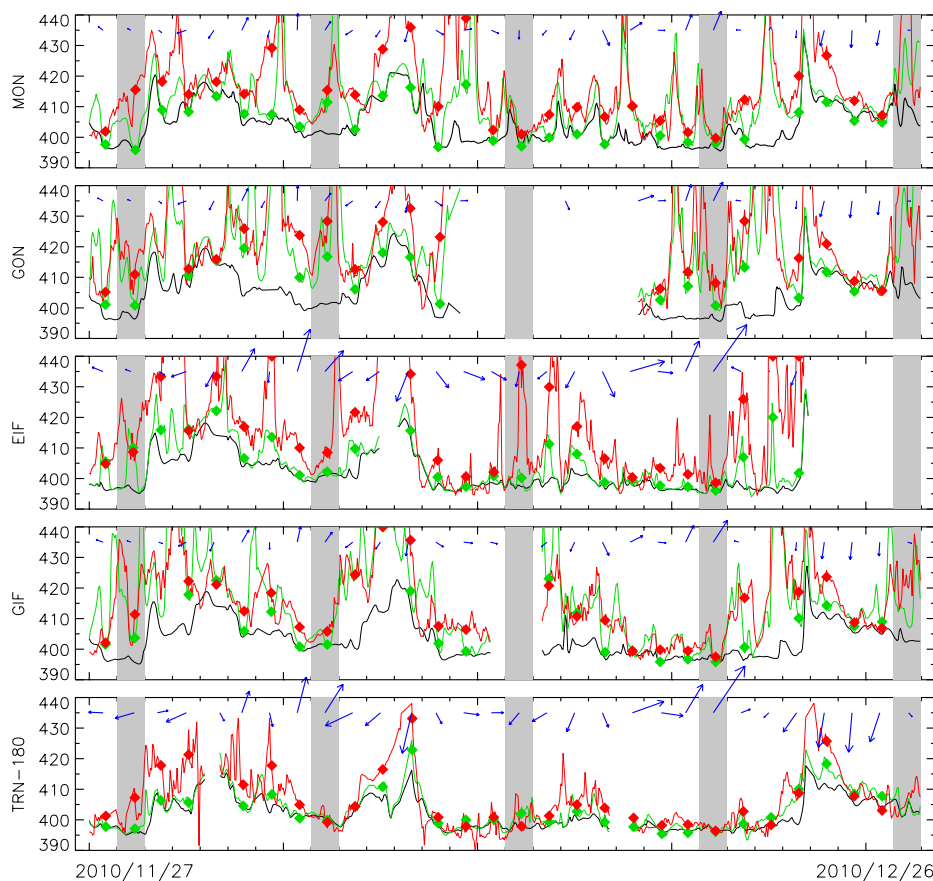


Figure 5: Time series of the measured (red) and modelled (green) CO₂ mole fraction [ppm] for the five sites used in this paper (See Table 1). The black line is the modelled mole fraction that is transported from the domain boundaries, with additional contribution from anthropogenic emissions outside the Île-de-France region (Edgar fluxes). The green line shows the modelled mole fraction that includes the same contributions, plus the biogenic fluxes within the modelling domain and the anthropogenic emissions within the Île-de-France region. Red are the observations. Note that there are some time periods when no measurements are available due to either calibration processes or, more rarely, failure of the monitoring instrumentation. For such periods, modelling results are not shown. The symbols show the mean of the afternoon measurement/model values that are used for the inversion. The blue arrows indicate the wind speed and direction at noon. A length equivalent to 1 day on the X-axis is for a wind speed of 10 m/s. [Grey shaded areas indicate Sundays.](#) This figure

is for the 30 days period starting on 2010/11/27. [Figure S1 in the supplementary shows the same figure for the other period.](#)

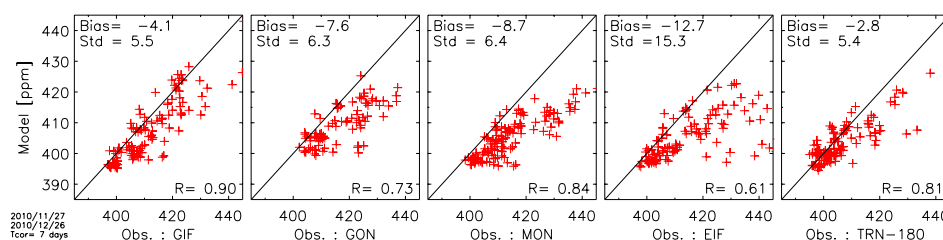


Figure 6 : Scatter plot of the measured and modelled CO₂ mole fractions at the 5 monitoring stations within and in the vicinity of the Paris city. The model vs measurement bias, standard deviation and correlations are provided within each subplot. This figure is for the 30 days period starting on 2010/11/27. [Figure S2 in the supplementary shows the same figure for the other period.](#)

FMB 20/1/2015 18:45
Deleted: Grey shaded areas indicate Sundays

FMB 20/1/2015 18:45
Deleted: Page Break
... [26]

FMB 20/1/2015 18:45
Moved down [9]: Daily flux estimates of the anthropogenic emission for the 30 days of the period. The blue line and shading shows the prior flux according to the AirParif inventory together with its assumed uncertainty. Yellow shading indicate Sundays; note the weekly cycle with lower values during Saturdays

FMB 20/1/2015 18:45
Deleted: Sundays. The red symbols

FMB 20/1/2015 18:45
Deleted: bars show the posterior estimates with their uncertainty range.

FMB 20/1/2015 18:45
Deleted: Nov-Dec period. A similar figure for the Oct-Nov period is shown

FMB 20/1/2015 18:45
Deleted: material

FMB 20/1/2015 18:45
Formatted: Font:Bold

FMB 20/1/2015 18:45
Deleted: ... [27]

FMB 20/1/2015 18:45
Formatted: Left

FMB 20/1/2015 18:45
Moved down [10]: Total flux estimates over the full 30 day period, for the 4 6-hour periods. Red is for the anthropogenic emissions, green is for the biogenic fluxes while blue is for the total. The prior estimates are shown as open rectangles while the posterior are shown as filled rectangles.

FMB 20/1/2015 18:45
Deleted: This figure is for the Nov-Dec period. A similar figure for the Oct-Nov period is shown in the supplementary material. ... [28]

FMB 20/1/2015 18:45
Moved down [11]: The second row shows the concentration estimates derived from the prior values for the biogenic fluxes and anthropogenic fluxes against the corre ... [29]

FMB 20/1/2015 18:45
Formatted: Default Paragraph Font

FMB 20/1/2015 18:45
Deleted: A similar figure for the Oct-Nov period is shown in the supplementary material.

FMB 20/1/2015 18:45
Formatted: Default Paragraph Font

FMB 20/1/2015 18:45
Formatted: Space Before: 0 pt, Line spacing: single

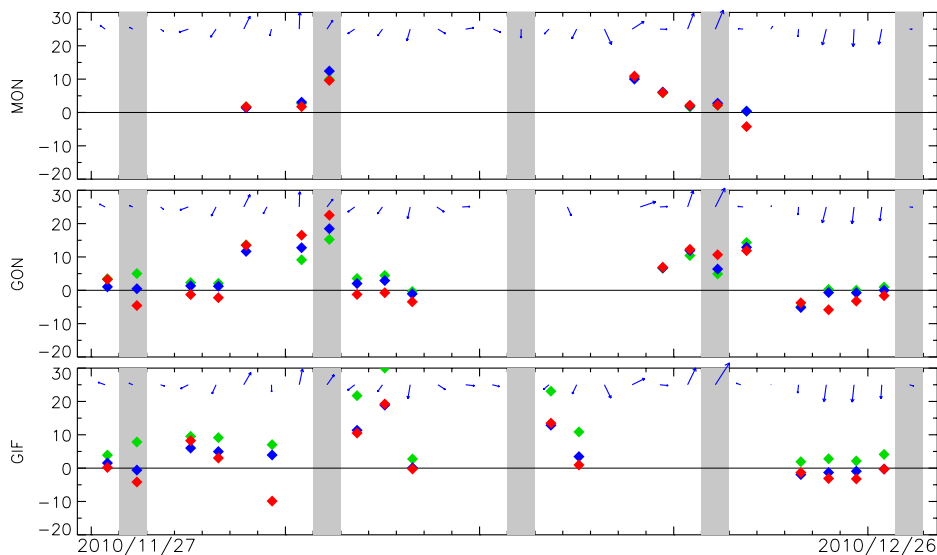


Figure 7: Time series of the mole fraction differences between a station (Y-axis label) and another one used as a reference (either GIF or GON) and selected based on the wind direction (see section 3.3). The symbols show the mean afternoon concentrations (12AM-4PM) for the measurements (red), the prior (green) and the posterior (blue) estimates. As in Figure 5, the arrows indicate the wind speed and direction. A similar figure for the other time period is shown in the supplementary material.

François-Marie Bréon 20/1/2015 18:46

Deleted: 97

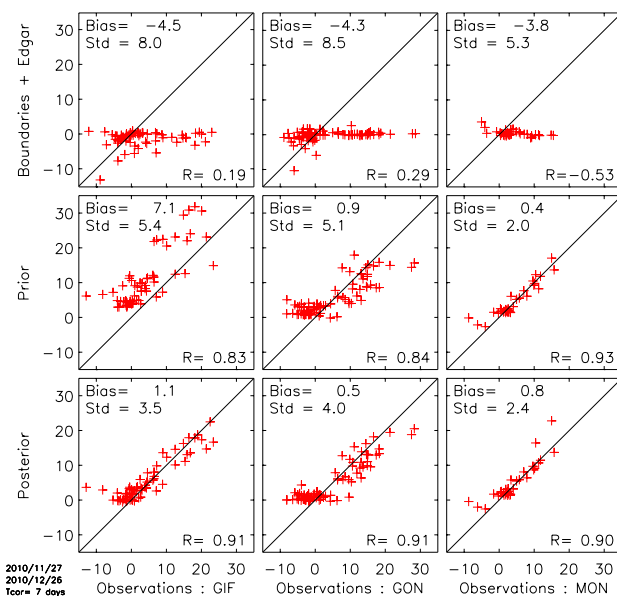


Figure 8: Scatter plot of the measured and modelled concentration gradients for 3 downwind stations; either GIF or MON are used as an upwind reference. The first row shows the mole fraction simulated using the boundary conditions and the anthropogenic emissions outside Île-de-France (y_F in equation 1) against the measurements. The second row shows the concentration estimates derived from the prior values for the biogenic fluxes and anthropogenic fluxes against the corrected measurements (i.e. $y - y_F$ in equation 1). The last row is the same but using the posterior estimates. This figure is for the Nov-Dec period. A similar figure for the other time period is shown in the supplementary material.

FMB 20/1/2015 18:45

2010/11/27
2010/12/26
Tcorr = 7 days

Deleted: François-Marie Bréon 20/1/2015 18:46
Deleted: 108

FMB 20/1/2015 18:45
Deleted: : Same as Figure 8 but

FMB 20/1/2015 18:45
Deleted: gradients where the reference

FMB 20/1/2015 18:45
Moved (insertion) [11]

FMB 20/1/2015 18:45
Formatted: Default Paragraph Font

FMB 20/1/2015 18:45
Deleted: is selected according to the wind direction. The TRN and EIF stations are not used.

1
2
3
4
5
6
7
8
9
10
11

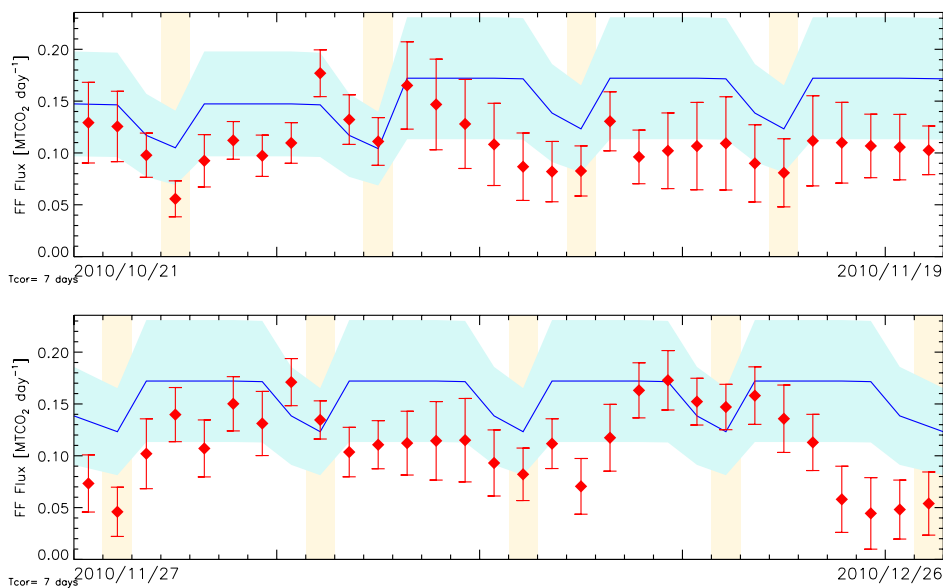


Figure 9.: Daily flux estimates of the anthropogenic emission for the 30 days of the period. The blue line and shading shows the prior flux according to the AirParif inventory together with its assumed uncertainty. Yellow shading indicate Sundays; note the weekly cycle with lower values during Saturdays and Sundays. The red symbols and bars show the posterior estimates with their uncertainty range. Both 30-day periods are shown.

FMB 20/1/2015 18:45
Moved (insertion) [9]

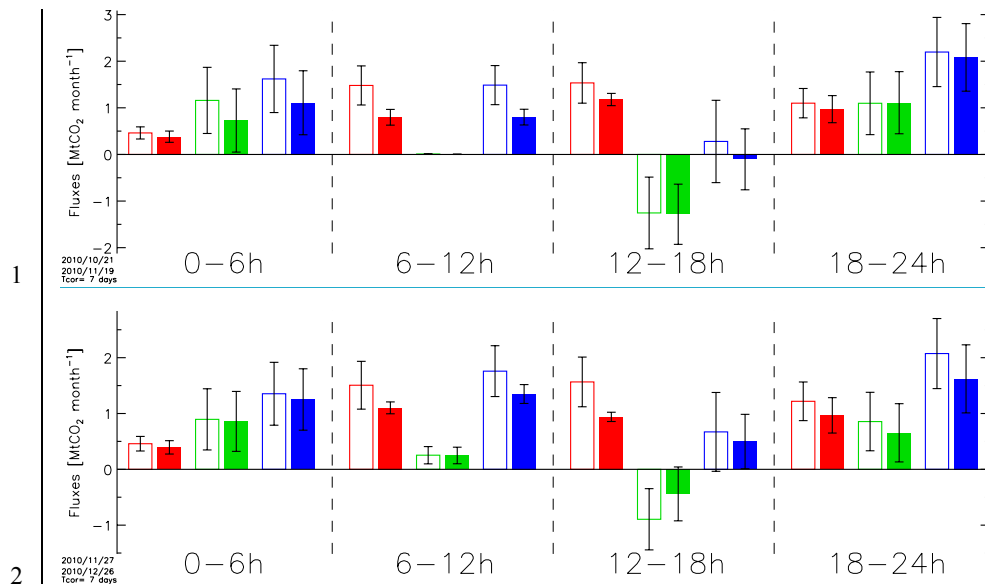


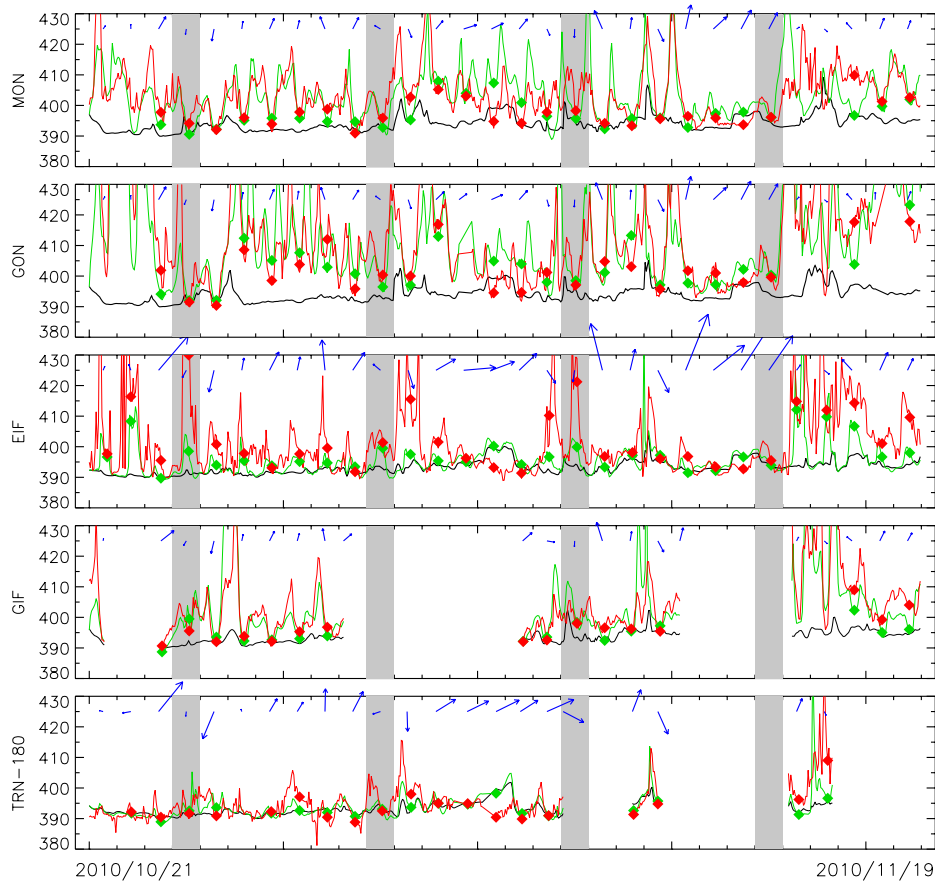
Figure 10.: Total flux estimates over the full 30 day period, for the 4 6-hour periods. Red is for the anthropogenic emissions, green is for the biogenic fluxes while blue is for the total. The prior estimates are shown as open rectangles while the posterior are shown as filled rectangles. Both 30-day periods are shown independently.

FMB 20/1/2015 18:45
Moved (insertion) [10]

FMB 20/1/2015 18:45
Deleted: Figure 11 : Same as Figure 6 but for the inversion based on the concentration gradients, and using only the three measuring stations in the vicinity of the Paris city. Both 30-day periods are shown. [30]

1 Supplementary material

2



3

4 Figure S- 1: Same as Figure 5 but for the 30 days period starting on October 21st.

5

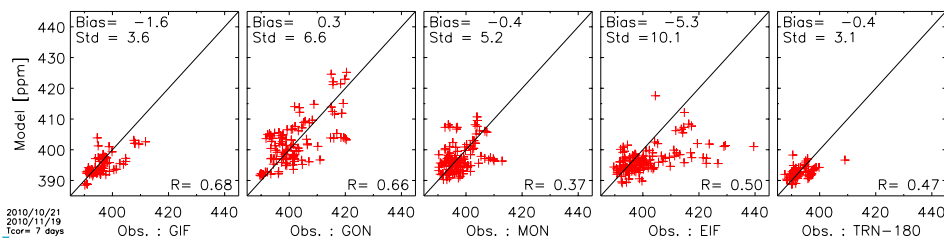


Figure S- 2 : Same as Figure 6 but for the 30 day period starting on October 21st.

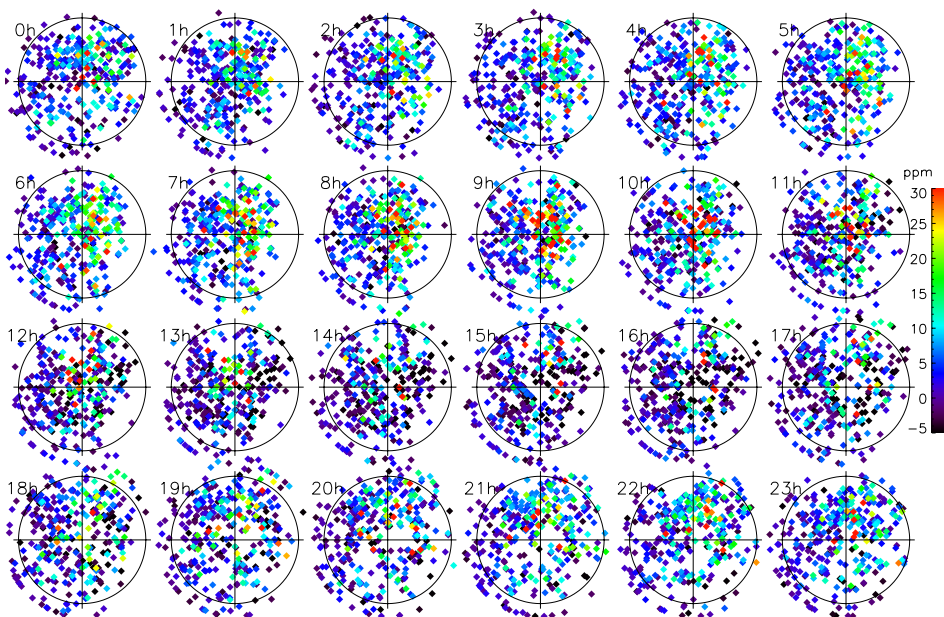
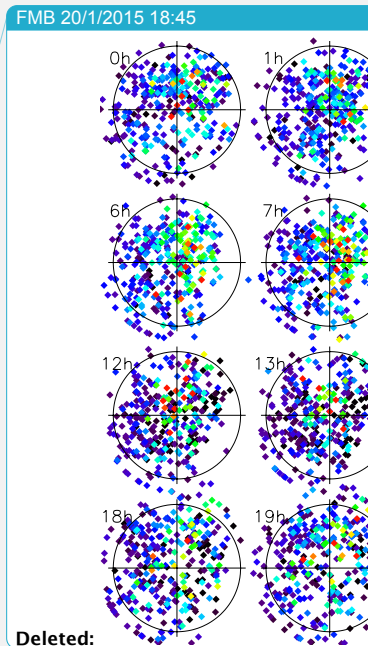


Figure S- 3 : Measurement-Model difference in CO₂ mole fraction at the EIF site as a function of time, wind speed and direction. The position of the symbols indicates the wind direction (top-right is for a wind from the North-East) and speed (the circles indicate a wind of 10 m s⁻¹). The wind speeds have been bounded at 12 m s⁻¹.



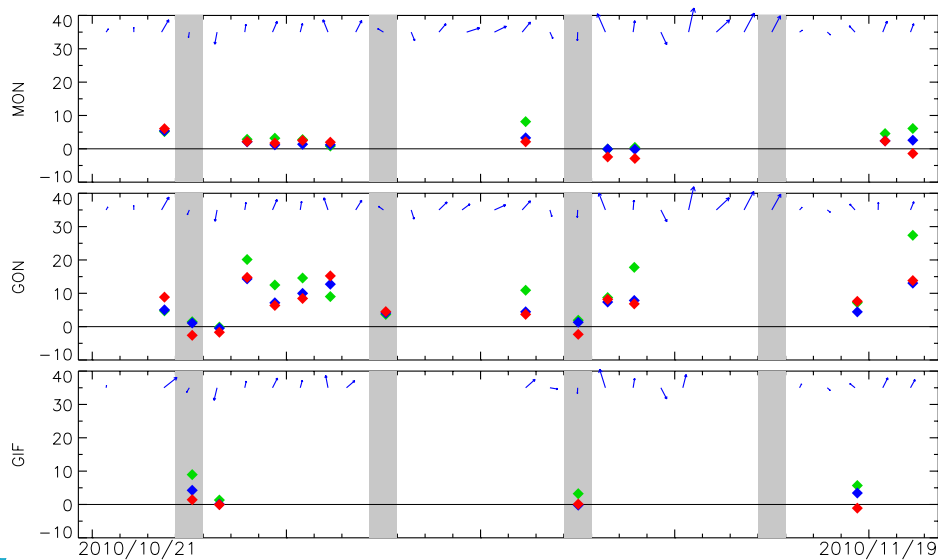


Figure S-4 : Same as Figure 7 but for the 30-day period starting on October 21st.

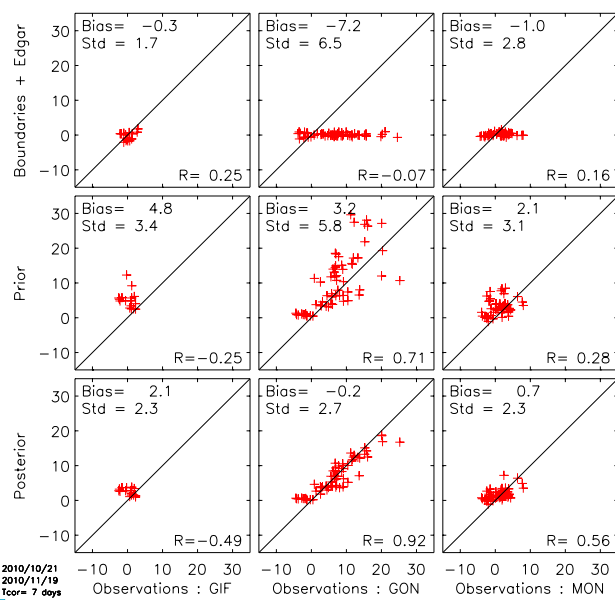


Figure S-5 : Same as Figure 8 but for the 30-day period starting on October 21st.

